AD_____

Award Number: DAMD17-03-1-0245

TITLE: Computerized Interpretation of Dynamic Breast MRI

PRINCIPLE INVESTIGATOR: Weijie Chen

CONTRACTING ORGANIZATION: University of Chicago
Chicago, IL 60637

REPORT DATE: May 2006

TYPE OF REPORT: Annual Summary

PREPARED FOR: U.S. Army Medical Research and Materiel Command
Fort Detrick, Maryland 21702-5012

DISTRIBUTION STATEMENT: Approved for Public Release;
Distribution Unlimited

REPORT DOCUMENTATION PAGE

Form Approved
OMB No. 0704-0188

1. REPORT DATE	2. REPORT TYPE	3. DATES COVERED
01-05-2006	Annual Summary	14 Apr 2003 – 13 Apr 2006

4. TITLE AND SUBTITLE

Computerized Interpretation of Dynamic Breast MRI

5a. CONTRACT NUMBER

5b. GRANT NUMBER
DAMD17-03-1-0245

5c. PROGRAM ELEMENT NUMBER

6. AUTHOR(S)

Weijie Chen

5d. PROJECT NUMBER

5e. TASK NUMBER

5f. WORK UNIT NUMBER

7. PERFORMING ORGANIZATION NAME(S) AND ADDRESS(ES)

University of Chicago
Chicago, IL 60637

8. PERFORMING ORGANIZATION REPORT NUMBER

9. SPONSORING / MONITORING AGENCY NAME(S) AND ADDRESS(ES)
U.S. Army Medical Research and Materiel Command
Fort Detrick, Maryland 21702-5012

10. SPONSOR/MONITOR'S ACRONYM(S)

11. SPONSOR/MONITOR'S REPORT NUMBER(S)

12. DISTRIBUTION / AVAILABILITY STATEMENT
Approved for Public Release; Distribution Unlimited

13. SUPPLEMENTARY NOTES
Original contains colored plates: ALL DTIC reproductions will be in black and white.

14. ABSTRACT

In the past three years, we have investigated computerized methods for analyses and interpretation of breast MR images. We investigated an automatic method for correcting intensity inhomogenieity artifacts in breast MR images. We developed a fuzzy c-means (FCM) based method for 3D lesion segmentation, which is a key procedure in computerized interpretation of breast MR images including differential diagnosis and assessment of response to therapy. The computerized segmentation yielded 97% of 121 lesions having overlap larger than 0.4 with an experienced radiologist's manual outlining. We investigated computerized methods for automatic identification of characteristic kinetic curves (CKC) from the segmented 3D lesion and automatic extraction of kinetic features from the identified CKCs. The automatic method significantly improved the performance of kinetic features in the task of distinguishing between malignant and benign lesions. We also investigated a volumetric texture analysis method for classifying breast lesions on MRI as malignant and benign. The 3D method was found to have significantly better classification performance than the traditional 2D method. Finally, we assessed the relative importance of the various features—kinetic, morphological, and texture—in differential diagnosis and combined multi-category features using a Bayesian neural network the performance of which was evaluated using two breast MR databases. Our research could potentially expedite the standardization of guidelines for interpretation of dynamic breast MRI of breast.

15. SUBJECT TERMS
Breast Cancer

16. SECURITY CLASSIFICATION OF:				18. NUMBER OF PAGES	19a. NAME OF RESPONSIBLE PERSON
a. REPORT	b. ABSTRACT	c. THIS PAGE			USAMRMC
U	U	U	UU	52	19b. TELEPHONE NUMBER *(include area code)*

Standard Form 298 (Rev. 8-98)
Prescribed by ANSI Std. Z39.18

Table of Contents

INTRODUCTION

In recent years, dynamic contrast-enhanced magnetic resonance imaging (DCE-MRI) of the breast has been increasingly used in the diagnosis of radiographically dense breasts, assessment of disease extent in the patient with newly diagnosed breast cancer, problem-solving applications for difficult diagnostic evaluations, for difficult diagnostic evaluations, for screening high risk women for early cancer detection, and on monitoring response to therapy. The promising potential of MRI in diagnosis of breast cancer, as a complementary modality to X-ray mammography, has been well recognized [1][2][3]. Despite its well-recognized utilities, however, the technique has not been introduced to routine clinical breast imaging. One of the most important obstacles has been the lack of standardization in terms of interpretation guidelines [2][4]. The reproducibility, effectiveness and relative significance of interpretation criteria in the literature are far from being well evaluated.

A typical DCE-MRI study acquires a substantial amount of four-dimensional (4D) functional data consisting of three spatial dimensions and one temporal dimension. Navigation and interpretation of this large amount of multidimensional data is labor-intensive and even challenging for radiologists. Automated image analysis aims to extract relevant information from 4D DCE-MRI data and improve the accuracy and consistency of image interpretation. Computerized methods have the potential to reduce the inter- and intra-observer variations, reduce the workload of the radiologist, and facilitate the image interpretation; thus, becoming increasingly important with the expanding clinical applications of breast MRI.

The purpose of the proposed research is to develop computerized methods to take full advantage of the wealth information that dynamic MRI offers to improve methods for the diagnosis and interpretation of breast MR images. The research involved investigation of automatic methods for image artifacts correction, tumor segmentation, extraction of computerized features that help distinguish between benign and malignant lesions, and classification. Our hypothesis was that investigation of advanced image analysis algorithms would improve the performance of existing conventional methods in the task of distinguishing between malignant and benign lesions and characterization of breast MR lesions.

Figure 1 shows our research scheme for the proposed research tasks. We have developed an automatic method for correcting intensity inhomogeneity artifacts. We also developed a computerized method for assessing tumor extent in 3D. The primary feature used for 3D tumor segmentation is the postcontrast enhancement vector. Tumor segmentation is a key procedure in computerized interpretation of breast MR images including differential diagnosis and assessment of response to therapy. We investigated computerized method for optimal extraction of kinetic features from DCE-MR images. We also investigated a volumetric texture analysis method for classifying breast lesions on MRI as malignant and benign. Finally, we assessed the relative importance of the various features—kinetic, morphological, and texture—in differential diagnosis and evaluated using two breast MR databases. We developed a computer workstation integrating our image analyses methods with a user-friendly graphical interface. Our research could potentially expedite the standardization of guidelines for interpretation of dynamic breast MRI of breast.

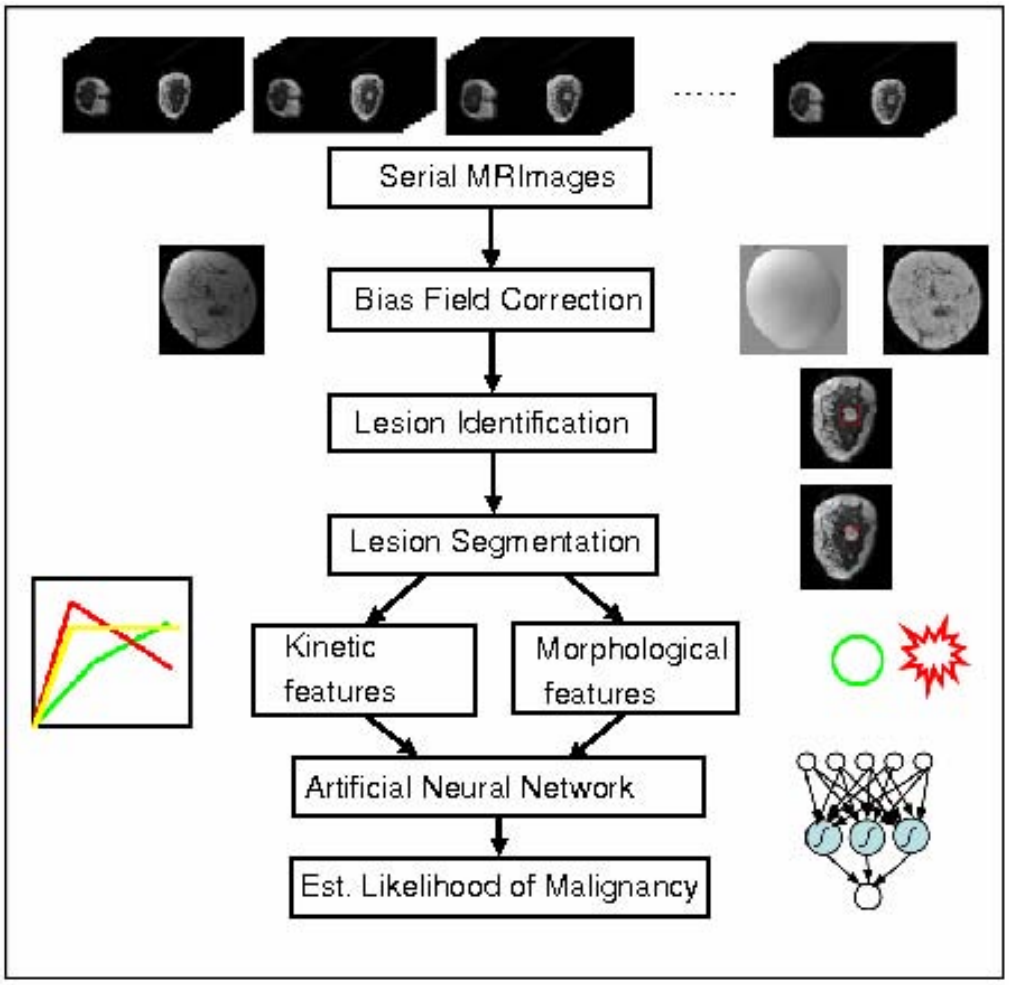

Figure 1. Diagram of our computerized scheme for breast MR image analysis and interpretation

BODY

Training Accomplishments

Weijie Chen, the recipient of the Predoctoral Traineeship Award has taken all the 22 required courses towards the Ph.D. degree in medical physics. The key courses included Physics of medical imaging (I & II), Physics of radiation therapy, Mathematics for medical physicists, Image processing, Statistics (I&II), Machine learning, Numerical computation, Topics in computer vision, Aanatomy of the body, Radiation biology, Beam physics, Clinical physics in PET, and Teaching assistant training.

Chen has passed his Ph.D. dissertation proposal last November, which is a critical step towards the Ph.D. degree as required by the Committee on Medical Physics, the University of Chicago. The Ph.D. dissertation is also under preparation.

Research Accomplishments

1. Database collection

The first part of our work has been collecting breast MR data. We have collected two databases. The first database contains dynamic breast MR images from 121 patients. Images were obtained using a T1-weighted 3D spoiled gradient echo sequence. After the acquisition of the precontrast series, Gd-DTPA contrast agent was injected intravenously by power injection with a dose of 0.2mmol/kg. Five postcontrast series were then taken with a time interval of 69 seconds. Each series contained 64 coronal slices with a matrix of 128 x256 pixels and an in-plane resolution of 1.25mm 1.25mm. Slice thickness ranged from 2 to 3 mm depending on breast size. For this database 121 primary mass lesions have been outlined by an experienced radiologist, 77 of the lesions are malignant and 44 lesions are benign, as revealed by biopsy.

We also collected over 200 patients' images data in the University of Chicago Hospitals. We have reviewed the images from the clinical site and excluded problematic cases (severe artifacts, missing data, biopsy unavailable). Case-review resulted 160 biopsy-proven lesions (109 malignant and 51 benign). These data were from a 1.5T GE scanner [temporal resolution of 72s; spatial resolution of 1.4 mm by 1.4 mm; slice thickness of 3 mm to 4 mm; Gd-DTPA dose of 0.1 mmol/kg].

2. Development of methods for shading artifacts correction in breast MR images

Most clinical MR images are corrupted by shading artifacts, which is slow intensity variations of the same tissue over the image domain. Such artifacts might affect computerized analysis such as tissue segmentation. We developed a FCM based approach that simultaneously estimates the shading effect while segmenting the image. A full description of the methods is in reference [5] which is attached as **Appendix A**. Further study will be done to investigate the influence of the shading artifacts on lesion extent assessment and on the performance of features in the task of distinguishing between malignant and benign lesions.

3. Investigation of image features

We used Database-I for investigation of features that contribute to the diagnosis of breast cancer. The lesions were delineated by an experienced radiologist as well as independently by computer using an automatic volume-growing algorithm. Fourteen features that were extracted automatically from the lesions could be grouped into three categories based on: (I) morphology; (II) enhancement kinetics; and (III) time course of enhancement-variation over the lesion. A stepwise feature selection procedure was employed to select an effective subset of features, which were then combined by linear discriminant analysis (LDA) into a discriminant score, related to the likelihood of malignancy. The classification performances of individual features and the combined discriminant score were evaluated with receiver operating characteristic (ROC) analysis. With the radiologist-delineated lesion contours, stepwise feature selection yielded 4 features and an A_z value of 0.80 for the LDA in leave-one-out cross-validation testing. With the computer-segmented lesion volumes, it yielded 6 features and an A_z value of 0.86 for the LDA in the leave-one-out testing. A full description of this study is given in reference [6] which is attached as **Appendix B**.

4. Investigation of methods for automatic tumor segmentation

We developed an automatic method for assessing tumor extent in 3D. The primary feature used for 3D tumor segmentation is the postcontrast enhancement vector. Tumor segmentation is a key procedure in computerized interpretation of breast MR images including differential diagnosis and assessment of response to therapy. This part of our research has been published [7] on ***Academic Radiology*** **16:63-72 (2006). (Appendix B)**

Accurate quantification of the shape and extent of breast tumors plays a vital role in nearly all applications of breast MR imaging, such as lesion characterization and assessment of tumor response to therapy. Specifically, tumor segmentation is a key component in the computerized assessment of likelihood of malignancy. However, manual delineation of lesions in 4-D MR images is labor intensive and subject to inter- and intra-observer variations. We developed a computerized lesion segmentation method that has the advantage of being automatic, efficient, and objective.

We developed a fuzzy c-means (FCM) clustering based method for the segmentation of breast lesions in 3-D from contrast-enhanced MR images. The proposed lesion segmentation algorithm consists of six consecutive stages: region of interest (ROI) selection by a human operator, lesion enhancement within the selected ROI, application of FCM on the enhanced ROI, binarization of the lesion membership map, connected-component labeling and object selection, and hole-filling on the selected object. We applied the algorithm to a clinical MR database consisting of 121 primary mass lesions. The manual segmentation of the lesions by an expert MR radiologist served as a reference in the evaluation of the computerized segmentation method. We also compared the proposed algorithm with a previously developed volume-growing (VG) method.

For the 121 mass lesions in our database, at an overlap threshold of 0.4, 97% lesions were correctly segmented by the proposed FCM based method while 84% lesions were correctly segmented by the VG method.

Our proposed algorithm for breast lesion segmentation in DCE-MRI was shown to be effective and efficient.

5. Automatic identification and classification of characteristic kinetic curves in breast MR lesions (published [8] on *Medical Physics* 33: 2878-2887 (2006), Appendix C.)

Dynamic contrast-enhanced magnetic resonance imaging (DCE-MRI) of the breast is being increasingly used in the detection and diagnosis of breast cancer as a complementary modality to mammography and sonography. Although the potential diagnostic value of kinetic curves in DCE-MRI is established, the method for generating kinetic curves is not standardized. The

inherent reason that curve identification is needed is that the uptake of contrast agent in a breast lesion is often heterogeneous, especially in malignant lesions. It is accepted that manual ROI selection in 4D breast MR images to generate the kinetic curve is a time-consuming process and suffers from significant inter- and intra- observer variability. We investigated and developed a fuzzy c-means (FCM) clustering based technique for automatically identifying characteristic kinetic curves from breast lesions in DCE-MRI of the breast. Dynamic contrast-enhanced MR images were obtained using a T1-weighted 3D spoiled gradient echo sequence with Gd-DTPA dose of 0.2 mmol/kg and temporal resolution of 69 s. FCM clustering was applied to automatically partition the signal-time curves in a segmented 3D breast lesion into a number of classes (ie, prototypic curves). The prototypic curve with the highest initial enhancement was selected as the representative characteristic kinetic curve (CKC) of the lesion. Four features were then extracted from each characteristic kinetic curve to depict the maximum contrast enhancement, time to peak, uptake rate and washout rate of the lesion kinetics. The performance of the kinetic features in the task of distinguishing between benign and malignant lesions was assessed by ROC analysis. With a database of 121 breast lesions (77 malignant and 44 benign cases), the classification performance of the FCM-identified CKCs was found to be better than that from the curves obtained by averaging over the entire lesion and similar to kinetic curves generated from regions drawn within the lesion by a radiologist experienced in breast MRI.

6. Volumetric texture analysis of DCE-MR images of the breast (presented [9] in ISMRM 2006)

Texture analysis using 2D-image-based gray level co-occurrence matrix method has been demonstrated to be useful in distinguishing between malignant and benign breast lesions in contrast-enhanced MR images. 2D texture analysis does not take advantage of the 3D data in breast MR images and requires extremely high signal-to-noise ratio, which may not be available in dynamic studies. We hypothesize that an overall assessment of texture on the accurately segmented 3D breast lesion would yield improved differentiation performance than 2D analysis. We extend the conventional 2D texture analysis technique to 3D in the framework of gray-level co-occurrence matrix method, and assess the performance of textural features in the task of distinguishing between malignant and benign breast lesions. For the 11 texture features under investigation, 7 features yielded statistically significant higher A_z values when 3D analyses were

used than when 2D analyses were used. We failed to find significant difference between 3D and 2D for the other four feautres Overall, texture analysis based on accurately segmented 3D lesions has improved diagnostic accuracy than that based on 2D ROIs.

7. Investigation of the computerized interpretation methods to expedite the standardization of guidelines for dynamic breast MRI of breast and evaluation of the relative importance of the various computer-extracted features. (Submitted to RSNA 2006)

Clinical breast MRI yields 4D datasets that are difficult in practice to manage and interpret. Our purpose is to develop a computerized system to aid the radiologist to better visualize and interpret breast MR images with automatic extraction of useful diagnostic information obtained in an effective and efficient manner.

Our analysis involved two breast MR databases totaling 281 biopsy-proven lesions. For each case, a T1-weighted SPGR sequence was used to acquire one precontrast and 5 postcontrast series. The first database (77 malignant and 44 benign) was obtained with a 1.5T Siemens scanner [temporal resolution of 69s; spatial resolution of 1.25 mm by 1.25 mm; slice thickness of 2 mm to 3 mm; Gd-DTPA dose of 0.2 mmol/km]. The second database (109 malignant and 51 benign) was from a 1.5T GE scanner [temporal resolution of 72s; spatial resolution of 1.4 mm by 1.4 mm; slice thickness of 3 mm to 4 mm; Gd-DTPA dose of 0.1 mmol/kg]. In our automatic method, the breast lesions initially undergo 3D segmentation by the computer. Then, the characteristic kinetic curves and the corresponding most-enhancing regions within the lesions are automatically identified. Lesion features are then automatically extracted and merged with a trained classifier to obtain the likelihood of malignancy. Such lesion features include (1) kinetic features that quantify the uptake and washout characteristics; (2) 3D texture features that quantify the uptake inhomogeneity; and (3) 3D shape descriptors that quantify the irregularity of the tumor.

The online computation time was approximately 15 seconds per case. Computer-segmentation agreed well with lesion outlines delineated by an experienced radiologist. In round-robin analysis, areas under the ROC curve of 0.88 and 0.82 were obtained for the first and second database, respectively, in the task of distinguishing between malignant and benign lesions.

The automatic computerized analyses of breast MR images yielded high interpretation performances for differential diagnosis, performance levels were similar across different MR scanners, and computation times were extremely short.

Our MRI-CAD system has potential to improve both the efficiency and effectiveness of breast MRI interpretation.

8. Development of a prototype workstation for computer-aided diagnosis (CAD) in contrast-enhanced MRI (RSNA 2005 InfoRAD Exhibit)

Computer-aided diagnosis (CAD) is a promising tool for assisting radiologist in diagnosing breast cancer on multi-modality breast images. With increasing applications of dynamic MRI in clinical breast imaging, CAD tool is expected to play a more significant role than it does in conventional modalities, as the amount of data in a typical dynamic study in breast MRI is huge and the data is 4-dimensional. We have developed a prototype CAD workstation (Figure 2) to aid the radiologist better visualize and interpret breast MR images. The workstation implements our state-of-the-art algorithms on lesion segmentation, feature extraction, and classification. With a user-friendly graphical-user-interface (GUI), the workstation enables visualization of multi-slice multi-series images simultaneously and the kinetic curve at a particular voxel can also be displayed. Breast mass lesions are segmented in 3-D automatically and efficiently from an operator-selected region of interest with a fuzzy c-means (FCM) based algorithm. Compared with careful manual delineation by an experienced radiologist, the automatic algorithm correctly segmented 97% of 121 mass lesions at overlap threshold 0.4. Characteristic kinetic curves are identified automatically from the segmented lesion with a FCM based method. The automatically identified kinetic curves performs significantly better than does the curves obtained by averaging over the entire lesion in the task of distinguishing between malignant and benign lesions ($p<0.00005$). Morphological features extracted from the segmented lesion and kinetic features extracted from the identified kinetic curves are merged by a classifier to estimate the likelihood of malignancy which is used to help radiologist in decision making.

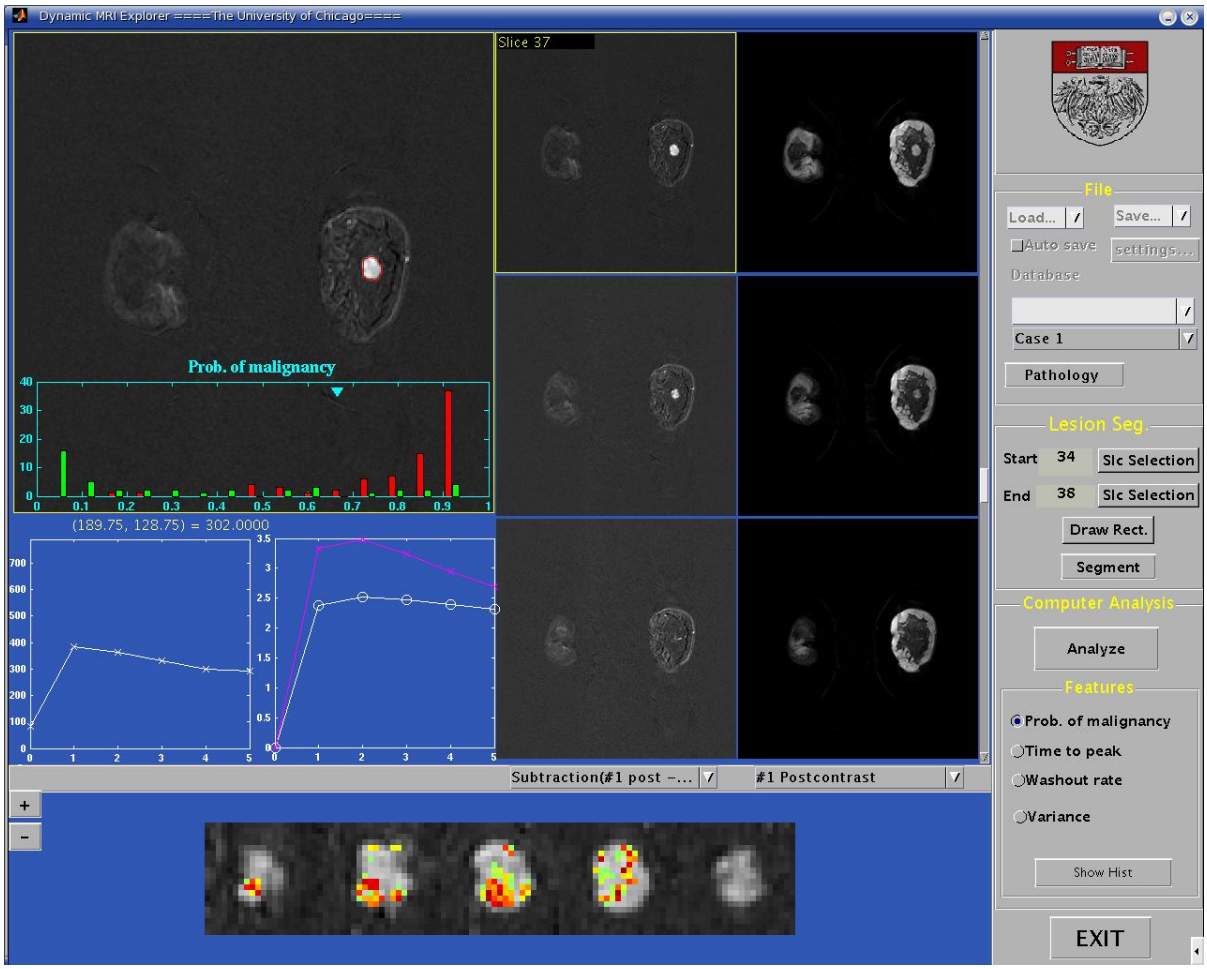

Figure 2: Graphical user interface (GUI) we developed for computerized image analysis in breast MRI

KEY RESEARCH ACCOMPLISHMENTS

- Collection and maintenance of clinical database: dynamic MR images of over 300 patients have been collected which are well suitable for the proposed research;
- Developed computerized methods for assessment of tumor extent which outperformed the previous region-growing method.
- Developed automatic methods for shading artifacts correction in breast MR images which will increase he performance of lesion features for diagnosis;
- Automatic identification and classification of characteristic kinetic curves in breast MR lesions: outperformed the performance of enhancement kinetics obtained from averaging over the entire lesion in the diagnosis of breast cancer and similar to or superior than manually drawn ROIs;
- Volumetric texture analysis of DCE-MR images of the breast: texture analysis based on accurately segmented 3D lesions has improved diagnostic accuracy than that based on 2D ROIs.
- Investigation of the computerized interpretation methods to expedite the standardization of guidelines for dynamic breast MRI of breast and evaluation of the relative importance of the various computer-extracted features;
- Development of a prototype workstation for computer-aided diagnosis (CAD) in contrast-enhanced MRI.

REPORTABLE OUTCOMES

Peer reviewed journal papers

- W. Chen**,** M. L. Giger, L. Lan, and U. Bick, "Computerized interpretation of breast MRI: Investigation of enhancement-variance dynamics," Medical Physics, 31:1076-1082, (2004).
- W. Chen, M. L. Giger, U. Bick. A fuzzy c-means (FCM) based approach for computerized segmentation of breast lesions in dynamic contrast-enhanced MR images. Academic Radiology 16:63-72 (2006).
- W. Chen, M. L. Giger, U. Bick, G. M. Newstead. Automatic identification and classification of characteristic kinetic curves of breast lesions on DCE-MRI. Medical Physics. 33:2878-2887 (2006)

Papers in conference proceedings

- W. Chen**,** M. L. Giger, and U. Bick, "Automated identification of temporal pattern with high initial enhancement in dynamic MR breast lesions using fuzzy c-means algorithm," *Proceedings SPIE,* 2004.
- W. Chen, M. L. Giger, "A fuzzy c-means (FCM) based algorithm for intensity inhomogeneity correction and segmentation of MR images," *Proceedings of IEEE International Symposium on Biomedical Imaging*, 2004.
- W.Chen, M.L.Giger, G. Newstead, U. Bick, L. Lan, "Computerized assessment of tumor extent in contrast-enhanced MR images of the breast," *Proceedings of 18th International Congress and Exhibition- Computer Assisted Radiology and Surgery, (CARS 2004), in press*
- W. Chen, M. L. Giger. A novel strategy for segmentation of magnetic resonance (MR) images corrupted by intensity inhomogeneity artifacts. Proceedings of SPIE, v 6144 I, Medical Imaging 2006: Image Processing, 2006, p 61441C
- W. Chen, M. L. Giger. Volumetric texture analysis of DCE-MRimages of the breast using gray-level co-occurrence matrix method. Proc. Intl. Soc. Mag. Reson. Med. (2006) p. 2885

Presentations

- W. Chen, M. L. Giger, and U. Bick, "Automated identification of temporal pattern with high initial enhancement in dynamic MR breast lesions using fuzzy c-means algorithm," SPIE-Medical Imaging, San Diego, California, February 2004.

- W. Chen, M. L. Giger, G. M. Newstead, U. Bick, L. Lan, "Computerized analysis of contrast-enhanced MR images of the breast: automated bias field correction and identification of characteristic signal-time curves," 90th Assembly and Annual Meeting of Radiological Society of North America, Chicago, Illinois, USA, December 2004.
- W. Chen, M. L.Giger, G. Newstead, U. Bick, L. Lan, "Dynamic MRI Explorer: A Prototype CAD Workstation for Diagnosis of Breast Cancer in Breast MRI", *info***RAD** Exhibit, 91th Assembly and Annual Meeting of Radiological Society of North America, Chicago, Illinois, USA, December 2005
- W. Chen, M. L. Giger. A novel strategy for segmentation of magnetic resonance (MR) images corrupted by intensity inhomogeneity artifacts. SPIE-Medical Imaging, San Diego, California, February 2006

Posters/Education Exhibits

- **W.Chen**, M.L.Giger, G. Newstead, U. Bick, L. Lan, "Computerized analysis of contrast-enhanced MR images of the breast: automated identification of signal-time curves," Era of Hope – Department of Defense Breast Cancer Research Program Meeting, Philadelphia, Pennsylvania, June 8-11, 2005

- **W.Chen**, M.L.Giger, G. Newstead, U. Bick, L. Lan, "Dynamic MRI Explorer: A Prototype CAD Workstation for Diagnosis of Breast Cancer in Breast MRI", *info***RAD** Exhibit, 91th Assembly and Annual Meeting of Radiological Society of North America, Chicago, Illinois, USA, December 2005

- **W. Chen**, M. L. Giger. Volumetric texture analysis of DCE-MR images of the breast using gray-level co-occurrence matrix method. ISMRM 14th Scientific Meeting, Seattle, Washington, USA 2006.

Awards

2006 Educational Stipend, International Society for Magnetic Resonance in Medicine (ISMRM)

2006 Recipient of Women's Board Travel Awards in the Division of the Biological Sciences for Winter/Spring 2006, the University of Chicago Women's Board

2005 Lawrence H. Lanzl Medical Physics Graduate Student Award, Department of Radiology and the Committee on Medical Physics, the University of Chicago

2004 Dolittle-Harrison Fellowship, The University of Chicago

CONCLUSIONS

The recipient of the Predoctoral Traineeship Award has taken all the required core courses and many research related elective courses as well. These trainings have proven useful for the recipient to achieve the proposed research goals. The goal of this grant was to support the recipient for research towards Ph.D. degree. The trainee has made excellent progress in this aspect, as he has passed his dissertation proposal, which is a key step to obtain Ph.D. degree in medical physics at the University of Chicago. He has finished the proposed research work and the dissertation is under preparation.

We have collected and maintained two dynamic breast MRI databases that are well suitable for the proposed research on computerized interpretation of breast MR images. We have developed computerized methods for correction of shading artifacts, tumor segmentation, and feature extraction and classification. The results have shown that our computerized analysis and interpretation methods have improved the existing methods significantly in the task of distinguishing between malignant and benign breast lesions on contrast-enhanced magnetic resonance images. The computerized scheme for breast MR image interpretation has great promise in increasing the objectivity, efficiency, and accuracy of the diagnosis of breast cancer.

Overall, we have well achieved the goals of the research proposal for the Predoctoral Traineeship Award.

REFERENCES

[1] G.M. Newstead, “Role of MR in Breast Imaging,” *RSNA Categorical Course in Breast Imaging*, 1999; pp287-293

[2] S.G. Orel and M.D. Schnall, “MR imaging of the breast for the detection, diagnosis, and staging of breast cancer,” Radiology, 220:13-30 (2001)

[3] S.E. Harms, D.P. Flamig, “Breast MRI”, Journal of clinical imaging, 25 (2001) 227-246

[4] C.K. Kuhl, and H.H. Schild, "Dynamic image interpretation of MRI of the breast," J. of Magn. Reson. Imaging, 12:965-974 (2000)

[5] W. Chen, M. L. Giger, “A fuzzy c-means (FCM) based algorithm for intensity inhomogeneity correction and segmentation of MR images,” *Proceedings of IEEE International Symposium on Biomedical Imaging*, 2004.

[6] W. Chen**,** M. L. Giger, L. Lan, and U. Bick, “Computerized interpretation of breast MRI: Investigation of enhancement-variance dynamics,” Medical Physics, 31:1076-1082, (2004).

[7] W. Chen, M. L. Giger, U. Bick. A fuzzy c-means (FCM) based approach for computerized segmentation of breast lesions in dynamic contrast-enhanced MR images. Academic Radiology 16:63-72 (2006).

[8] W. Chen, M. L. Giger, U. Bick, G. M. Newstead. Automatic identification and classification of characteristic kinetic curves of breast lesions on DCE-MRI. Medical Physics. 33:2878-2887 (2006)

[9] W. Chen, M. L. Giger. Volumetric texture analysis of DCE-MRimages of the breast using gray-level co-occurrence matrix method. Proc. Intl. Soc. Mag. Reson. Med. (2006) p. 2885

APPENDICS

Appendix A.

[5] W. Chen, M. L. Giger, "A fuzzy c-means (FCM) based algorithm for intensity inhomogeneity correction and segmentation of MR images," *Proceedings of IEEE International Symposium on Biomedical Imaging*, 2004.

Appendix B.

[6] W. Chen**,** M. L. Giger, L. Lan, and U. Bick, "Computerized interpretation of breast MRI: Investigation of enhancement-variance dynamics," Medical Physics, 31:1076-1082, (2004).

Appendix C.

[7] W. Chen, M. L. Giger, U. Bick. A fuzzy c-means (FCM) based approach for computerized segmentation of breast lesions in dynamic contrast-enhanced MR images. Academic Radiology 16:63-72 (2006).

Appendix D.

[8] W. Chen, M. L. Giger, U. Bick, G. M. Newstead. Automatic identification and classification of characteristic kinetic curves of breast lesions on DCE-MRI. Medical Physics. 33:2878-2887 (2006)

Appendix E.

[9] W. Chen, M. L. Giger. Volumetric texture analysis of DCE-MRimages of the breast using gray-level co-occurrence matrix method. Proc. Intl. Soc. Mag. Reson. Med. (2006) p. 2885

A fuzzy c-means (FCM) based algorithm for intensity inhomogeneity correction and segmentation of MR images

Weijie Chen
Dept. of Radiology
The University of Chicago
Chicago,IL 60637
Email: weijie@uchicago.edu

Maryellen L. Giger
Dept. of Radiology
The University of Chicago
Chicago,IL 60637
Email: m-giger@uchicago.edu

***Abstract*— Magnetic resonance images are often corrupted by intensity inhomogeneity, which manifests itself as slow intensity variations of the same tissue over the image domain. Such shading artifacts must be corrected before doing computerized analysis such as intensity-based segmentation and quantitative analysis. In this paper, we present a fuzzy c-means (FCM) based algorithm that simultaneously estimates the shading effect while segmenting the image. A multiplier field term that models the intensity variation is incorporated into the FCM objective function which is minimized iteratively. In each iteration, the bias field is estimated based on the current tissue class centroids and the membership values of the voxels and then smoothed by an iterative low-pass filter. The efficacy of the algorithm is demonstrated on clinical breast MR images.**

I. Introduction

Magnetic resonance imaging (MRI) has many advantages over other diagnostic imaging modalities, such as high contrast between soft tissues, high spatial resolution and inherent 3D nature, thus has gained wide clinical applications. Breast MRI, for example, has been widely investigated in the past decade in the detection and diagnosis of breast cancer as a complementary modality to X-ray mammography[1], in assessment of the localization and extent of breast lesions[2], and in monitoring tumor response to therapy[3]. Furthermore, breast MRI can be used for quantitative assessment of fibroglandular tissue percentage[4] which is a predictor of breast cancer risk. While qualitative visual assessment is often used by radiologists in a clinical environment, computerized quantitative analysis is increasingly needed to aid the radiologists increase both the accuracy and the efficiency of the diagnosis.

Magnetic resonance images are often corrupted by intensity inhomogeneity, which manifests itself as slow intensity variations of the same tissue over the image domain[5]. Such shading artifacts is the major source of difficulty for computerized analysis such as intensity-based segmentation and quantitative analysis. A number of algorithms have been proposed for the correction of spatial intensity inhomogeneity. Wells *et al.*[6], Guillemaud and Brady[7] developed a statistical approach based on the expectation-maximization (EM) algorithm that simultaneously estimates the bias field and segments the image into different tissue classes. Their methods yielded impressive results on brain MR images but has the disadvantage of being computationally intensive and requiring prior knowledge on intensity distributions of different tissue classes. Pham and Prince[8] proposed an adaptive fuzzy c-means (AFCM) algorithm for fuzzy segmentation of images while compensating for intensity inhomogeneities. AFCM is robust in convergence because the objective function to be minimized has regularization terms that ensure the estimated bias field is smooth and slowly varying. Ahmed *et al.*[9] proposed a bias-correction fuzzy c-means (BCFCM) algorithm in which they incorporated a neighborhood regularizer into the FCM objective function to allow labeling of a voxel to be influenced by the labels in its immediate neighborhood, making the algorithm insensitive to salt and peppernoise. However, they failed to address that the algorithm may converge to unwanted results without any constraint on the bias field. Li *et al.*[10] combined the AFCM and the neighborhood regularizer in BCFCM and obtained promising results in images with high noise level. The AFCM based methods, however, are computationally intensive and faster algorithm is needed in real-time clinical applications.

In this paper, we present a fast fuzzy c-means (FCM) based algorithm that simultaneously estimates the bias field while segmenting the image. A multiplier field term that models the intensity variation is incorporated into the FCM objective function which is minimized iteratively. In each iteration, the bias field is estimated based on the current tissue class centroids and the membership values of the voxels and then smoothed by an iterative low-pass filter. The efficacy of the algorithm is demonstrated on clinical breast MR images.

II. Methods

A. Bias field model

The observed MRI signal intensity is modeled as the "true" signal intensity multiplied by a spatially-varying factor called *gain* field, namely,

$$Y_i = X_i G_i \qquad \forall \quad i \in \{1, 2, \ldots, N\} \tag{1}$$

where Y_i, X_i, and G_i are the observed intensity, true intensity, and *gain* field at the *i*th voxel, respectively. N is the total number of voxels in the MR image. The artifact can be modeled as an additive *bias* field by applying a logarithmic transformation to both sides of (1)[6]

$$y_i = x_i + \beta_i \qquad \forall \quad i \in \{1, 2, \ldots, N\} \tag{2}$$

where y_i, x_i are the observed and true log-transformed intensities at the *i*th voxel, respectively, and β_i is the bias field at the *i*th voxel. By incorporating the bias field model into a fuzzy c-mean framework, we will be able to iteratively estimate both the true intensity and the bias field from the observed intensity.

B. Algorithm

In the image segmentation context, the standard FCM algorithm[11] is an optimization problem for partitioning an image of N voxels, $X = \{x_i\}_{i=1}^N$, into c (tissue) classes

$$\min_{U,V} \quad \{J(U, V; X) = \sum_{k=1}^{c} \sum_{i=1}^{N} u_{ki}^p \|x_i - v_k\|^2\} \tag{3}$$

subject to:

$$\sum_{k=1}^{c} u_{ki} = 1 \quad \forall i$$

$$0 \leq u_{ki} \leq 1 \quad \forall k, i$$

where U is the *partition matrix* whose element u_{ki} is the *membership* of the *i*th voxel for *k*th class. V is the *centroid* vector whose element v_k is the centroid (or prototype) of *k*th class. The parameter p, called *fuzzy index*, is a weighting exponent on each fuzzy membership and determines the amount of "fuziness" of the resulting partition. The norm operator $\|\cdot\|$ represents the standard Euclidean distance. The objective function J is minimized when high membership values are assigned to the pixels whose intensities are close to the centroid of its particular class, and low membership values are assigned to the voxels whose intensities are far from the centroid.

To incorporate the bias field into the FCM framework, we substitute (2) into (3). Then the fuzzy segmentation with the presence of bias field becomes a constrained optimization problem

$$\min_{U,V,B} \quad \{J_b(U, V, B; Y) = \sum_{k=1}^{c} \sum_{i=1}^{N} u_{ki}^p \|y_i - \beta_i - v_k\|^2\} \tag{4}$$

subject to:

$$\sum_{k=1}^{c} u_{ki} = 1 \quad \forall i$$

$$0 \leq u_{ki} \leq 1 \quad \forall k, i$$

where $Y = \{y_i\}_{i=1}^N$ is the observed image, $B = \{\beta_i\}_{i=1}^N$ is the bias field image.

To solve (4), we take the first derivatives of J_b with respect to u_{ki}, v_k, and β_k and setting them equal to zero. We thus obtain three necessary conditions for J_b to be at a minimum.

$$u_{ki}^* = \frac{1}{\sum_{l=1}^{c} (\frac{\|y_i - \beta_i - v_k\|}{\|y_i - \beta_i - v_l\|})^{2/(p-1)}} \tag{5}$$

$$v_k^* = \frac{\sum_{i=1}^{N} u_{ki}^p (y_i - \beta_i)}{\sum_{i=1}^{N} u_{ki}^p} \tag{6}$$

$$\beta_i^* = y_i - \frac{\sum_{k=1}^{c} u_{ki}^p v_k}{\sum_{k=1}^{c} u_{ki}^p} \tag{7}$$

From the first eye, an iterative scheme for minimizing the objective function J_b is straightforward by performing Picard iteration through the above three necessary conditions for (4) to be minimized. This is not the whole story, however, because B obtained from (7) is a "residual" image but not necessarily be the bias field image. A residual image could always be found that would set J_b to zero. Pham and Prince's AFCM algorithm solved the problem by introducing regularization terms into the objective function that ensure the resulted bias field image being smooth. The regularization terms, however, make the estimation of the bias field a computationally intensive process. Another solution is that we estimate the bias field by filtering the residual image B in (7) using an iterative low-pass spatial filter. This filtering strategy is based on the fact that the bias field is of low spatial frequency and the assumption that other components in the residual image is of higher frequency. The steps for our algorithm can then be described as the following:

1) Initialize class centroid values, $\{v_k\}_{k=1}^c$. Initialize $\{\beta_i\}_{i=1}^N$ with zeros.
2) Update partition matrix U using (5).
3) Update class centroids V using (6).
4) Estimate residual image using (7).
5) Filter the residual image using an iterative low-pass filter.
6) Go to Step 2 unless the following termination criterion is satisfied:
$$\|V_{new} - V_{old}\| < \epsilon \tag{8}$$
where ϵ is a user-chosen threshold.

III. Results

In this section we demonstrate the efficacy of our algorithm by applying it to clinical breast MR images. The images were obtained using a General Electric Signa 1.5-Tesla clinical MR scanner. We set the parameter *fuzzy index* $p = 2$, the termination criterion $\epsilon = 0.001$. The images were thresholded before analysis so that only tissues of interest were included in the computation and the background was excluded. We set the number of classes $c = 2$.

Fig.1(a) shows a clinical MR image corrupted by intensity inhomogeneity. Fig. 1(b) shows the estimated bias field using our algorithm and Fig.1(c) shows the corrected image using the bias field in (b). The membership map for dense tissue class is shown in Fig.1(d). Applying standard FCM algorithm

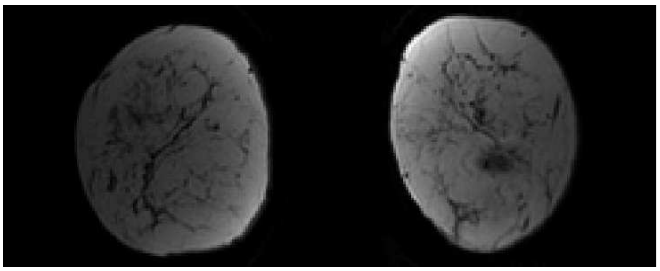

(a)

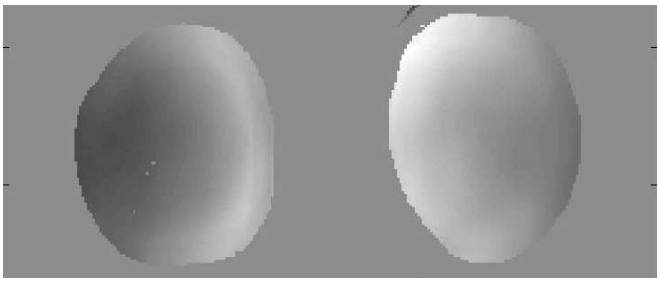

(b)

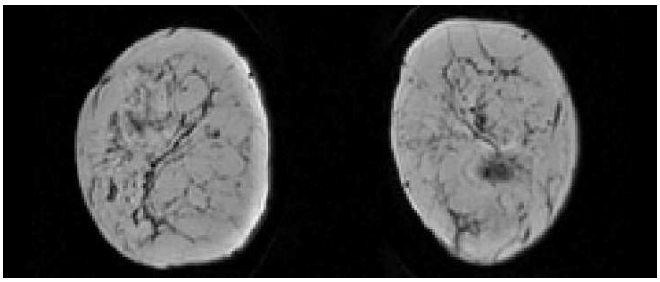

(c)

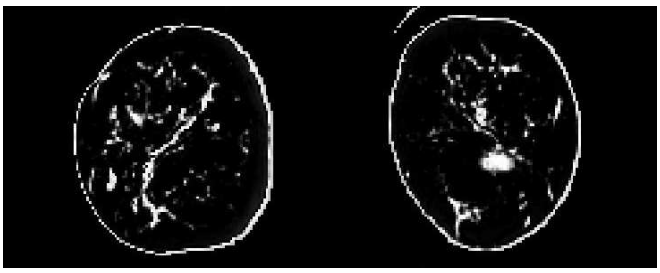

(d)

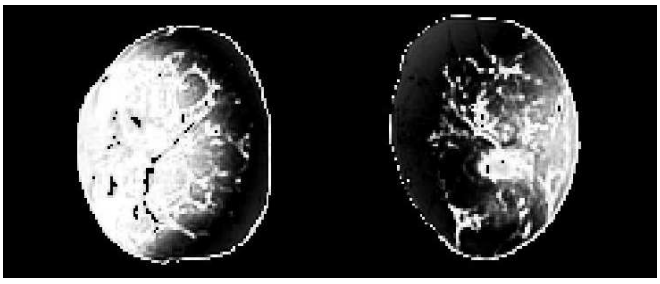

(e)

Fig. 1. Application of the proposed algorithm to a clinical breast MR image: (a)The original image. (b) Estimated bias field. (c) Corrected image. (d) The membership map for the dense-tissue class. (e) For comparison, the membership mapping from the standard FCM algorithm.

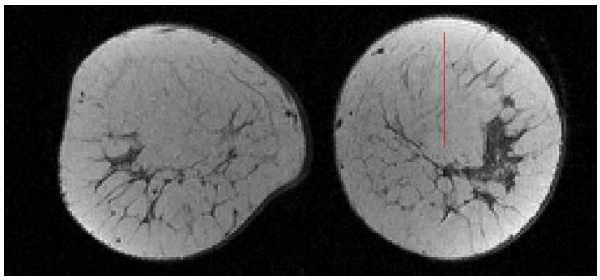

(a)

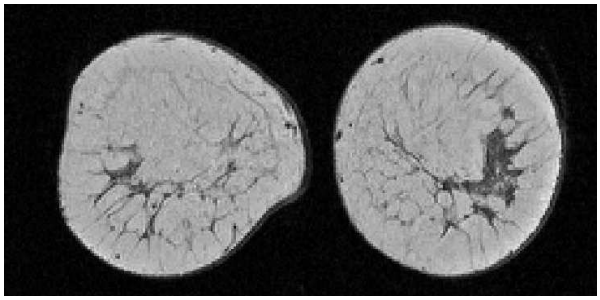

(b)

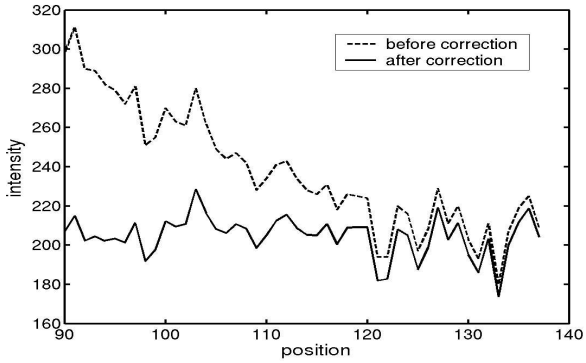

(c)

Fig. 2. Clinical breast MRI example: (a)The orginal image. (b) Corrected image. (c)The intensity profiles of a fat area as marked by a line in (a), for both the original and the bias corrected images.

to original image (a) without considering the bias field effect yielded a membership map shown in Fig.1(e). Apparently, intensity-based segmentation could not correctly segment the image without intensity inhomogeneity correction. By visual evaluation, our algorithm correctly estimated the bias field and dramatically improved the image quality and segmentation accuracy.

Fig.2 presents another breast MRI example. Fig.2(a) and (b) are the original and bias corrected images, respectively. We selected an area mainly consisting of fat tissue and plotted the intensity profiles for both the original and the bias corrected images, as shown in Fig.2(c). From the intensity profile of the original image, we can see that the intensity inhomogeneity in our clinical database can be as large as 40%. From the corrected intensity profile, the algorithm has successfully removed the bias field.

In both examples shown above, the algorithm converged

within 1-2 seconds on a PC AMD Athlon with 1.2 GHz CPU speed.

IV. Discussion

We are developing a computer-aided diagnosis (CAD) system for breast MR imaging. Bias field correction is a necessary preprocessing step for subsequent computerized quantitative analysis. And since the CAD system will ultimately be used in a clinical environment,it must run efficiently. Due to the high spatial resolution and 3-D nature of MR images, we are also using MR images to estimate the percentage of dense tissues in the whole breast, which is an indicator for breast cancer risk. The risk assessment application requires segmentation of the images into different tissue classes in the presence of intensity homogeneity. All these applications motivated us to develop a reliable, fast, and robust algorithm to solve the bias field correction problem.

Our preliminary experiences with the proposed algorithm showed that it is a promising method for intensity inhomogeneity correction and fuzzy segmentation of MR images. Our work in progress includes optimization of the current implementation and evaluation of the method with more data. The noise sensitivity of the algorithm will also be investigated and the neighborhood regularizer as proposed by Ahmed[9] might be incorporated into the current framework to improve the segmentation accuracy on noisy images. Finally, the current version of algorithm works for 2-D images and it is straightforward to generalize to 3-D images.

V. Conclusion

We have presented a fast algorithm based on FCM for intensity inhomogeneity correction and segmentation of MR images. The algorithm was formulated by introducing the bias field model into the FCM objective function which is then minimized iteratively. In each iteration step, the bias field was estimated based on the current tissue class centroids and the membership values of the voxels and then smoothed by an iterative mean filter. The efficacy of the algorithm is demonstrated on clinical breast MR images.

Acknowledgment

The research was supported by DOD Breast Cancer Research Program DAMD17-03-1-0245 and USPHS grant CA89452. M. L. Giger is a shareholder in R2 Technology, Sunnyvale, CA. It is the policy of the University of Chicago that investigators disclose publicly actual or potential significant financial interests that may appear to be affected by the research activities.

References

[1] J. C. Weinreb, G. Newstead,"MR imaging of the breast," *Radiology*,196(3), pp. 593-610, Sept. 1995.

[2] W. M. Kristoffersen, P. Aspelin, M. Sylvan, and B. Bone, "Comparison of lesion size estimated by dynamic MR imaging, mammography and histopathology in breast neoplasms," *Eur Radiol.*,13(6), pp. 1207-12, June 2003.

[3] K. Turetschek, A. Preda, E. Floyd, D. M. Shames, V. Novikov,T. P. Roberts, J. M. Wood, Y. Fu, W. D. Carter, and R. C. Brasch, "MRI monitoring of tumor response following angiogenesis inhibition in an experimental human breast cancer model," *Eur J Nucl Med Mol Imaging*,30(3), pp. 448-55, Mar 2003.

[4] N. A. Lee, H. Rusinek, J. Weinreb, R. Chandra, H. Toth, C. Singer, G. Newstead, "Fatty and fibroglandular tissue volumes in the breasts of women 20-83 years old: comparison of X-ray mammography and computer-assisted MR imaging," *Am J Roentgenol.*, 168(2), pp. 501-6,Feb. 1997.

[5] B. R. Condon, J. Patterson, and D. Wyper, "Image nonuniformity in magnetic resonance imaging: Its magnitude and methods for its correction," *Br. J. Radiol.*, vol. 60, pp. 83-87, 1987.

[6] W. M. Wells, III, W. E. L.Grimson, R.Kikinis, and F. A.Jolesz, "Adaptive segmentation of MRI data," *IEEE Trans. Med. Imag.*, vol. 15, pp. 429-442, Aug. 1996.

[7] R. Guillemaud and M.Brady, "Estimating the bias field of MR images," *IEEE Trans. Med. Imag.*, vol. 16, pp. 238-251, June 1997.

[8] D. L. Pham and J. L. Prince, "Adaptive fuzzy segmentation of magnetic resonance images," *IEEE Trans. Med. Imag.*, vol. 18, pp. 737-752, Sept. 1999.

[9] M. N. Ahmed, S. M. Yamany, N. Mohamed, A. A. Farag, and T. Moriarty,"A modified fuzzy c-means algorithm for bias field estimation and segmentation of MRI data," *IEEE Trans. Med. Imag.*, vol. 21, pp. 193-199, Mar. 2002.

[10] X. Li, L. Li, H. Lu, D. Chen, and Z. Liang, "Inhomogeneity correction for magnetic resonance images with fuzzy c-means algorithm," *Proc. SPIE*,Vol. 5032,Medical Imaging 2003: Image Processing, San Diego, CA, Feb. 2003, pp. 995-1005.

[11] J. Bezdek, L. Hall, and L. Clarke, "Review of MR image segmentation using pattern recognition," *Med. Phys.*, vol. 20, pp. 1033-1948, 1993.

Computerized interpretation of breast MRI: Investigation of enhancement-variance dynamics[a)]

Weijie Chen, Maryellen L. Giger,[b)] Li Lan, and Ulrich Bick
Department of Radiology, The University of Chicago, MC 2026, 5841 South Maryland Avenue, Chicago, Illinois 60637

(Received 23 July 2003; revised 12 February 2004; accepted for publication 13 February 2004; published 8 April 2004)

The advantages of breast MRI using contrast agent Gd-DTPA in the diagnosis of breast cancer have been well established. The variation of interpretation criteria and absence of interpretation guidelines, however, is a major obstacle for applications of MRI in the routine clinical practice of breast imaging. Our study aims to increase the objectivity and reproducibility of breast MRI interpretation by developing an automated interpretation approach for ultimate use in computer-aided diagnosis. The database in this study contains 121 cases: 77 malignant and 44 benign masses as revealed by biopsy. Images were obtained using a T1-weighted 3D spoiled gradient echo sequence. After the acquisition of the precontrast series, Gd-DTPA contrast agent was injected intravenously by power injection with a dose of 0.2 mmol/kg. Five postcontrast series were then taken with a time interval of 60 s. Each series contained 64 coronal slices with a matrix of 128×256 pixels and an in-plane resolution of $1.25\times1.25\ \mathrm{mm}^2$. Slice thickness ranged from 2 to 3 mm depending on breast size. The lesions were delineated by an experienced radiologist as well as independently by computer using an automatic volume-growing algorithm. Fourteen features that were extracted automatically from the lesions could be grouped into three categories based on (I) morphology, (II) enhancement kinetics, and (III) time course of enhancement-variation over the lesion. A stepwise feature selection procedure was employed to select an effective subset of features, which were then combined by linear discriminant analysis (LDA) into a discriminant score, related to the likelihood of malignancy. The classification performances of individual features and the combined discriminant score were evaluated with receiver operating characteristic (ROC) analysis. With the radiologist-delineated lesion contours, stepwise feature selection yielded four features and an A_z value of 0.80 for the LDA in leave-one-out cross-validation testing. With the computer-segmented lesion volumes, it yielded six features and an A_z value of 0.86 for the LDA in the leave-one-out testing. [DOI: 10.1118/1.1695652]

Key words: breast cancer, contrast-enhanced MRI, Gd-DTPA, computer-aided diagnosis (CAD), ROC analysis

I. INTRODUCTION

Breast MRI has emerged as a promising modality for the detection and diagnosis of breast cancer since the introduction of gadolinium-diethylenetriamine penta-acetic acid (Gd-DTPA) as a contrast agent.[1–3] Contrast-enhanced MRI (CE-MRI) allows lesions to be distinguished from normal tissues due to the increased vascularity and capillary permeability of tumors. CE-MRI offers three-dimensional spatial information and temporal information of breast cancer, qualifying it as an encouraging complementary modality to conventional imaging methods, such as x-ray mammography and sonography.

Despite its well-recognized advantages, applications of MRI in the routine clinical practice of breast imaging are limited. One of the most important obstacles is the lack of interpretation guidelines;[4,5] very few attempts have been made to standardize the interpretation of breast MR images. Among the few efforts in this regard is the work of the International Working Group on Breast MRI, which has developed and validated a detailed lexicon for breast MRI interpretation.[6] Investigators use a large variety of diagnostic criteria[2,3,7–13] that help classify lesions as benign or malignant. The interpretation criteria in the current literature fall into two major categories:[5,14] morphologic features[8,9,13] and enhancement kinetics,[2,3,12] i.e., the time course of signal intensity within the suspected lesions. While the studies using these criteria have shown promising results (sensitivity from 92% to 100%, specificity from 53% to 100%) as reported in a recent review,[15] significant variation does exist. The variation of the results may be due to two reasons from the interpretation aspect; one is the interobserver variation from different subjective judgments,[16–18] and the other is that the current interpretation schemes might not be sufficiently robust.

The aim of computerized interpretation of medical images is to obtain quantitative indices of malignancy. It has the advantage of being objective, automatic, and, furthermore, it may provide unique information that might be difficult to assess visually, especially for time-series 3D MR images.

This study aims to use computerized methods to investigate the potential of enhancement-variance dynamics in the interpretation of contrast-enhanced breast MR images. Auto-

matically extracted features are based on the time course of enhancement-variance within lesions. Features based on enhancement kinetics and morphology of lesions are studied as well for comparison. Also compared are the performances of features extracted from lesions delineated by experienced radiologist and those from lesions segmented by the computer using a volume-growing algorithm. Finally, different features are selected and merged into an estimate of malignancy using automated classification.

II. MATERIALS AND METHODS

A. Image database

The database in this study contains 121 cases: 77 malignant and 44 benign masses as revealed by biopsy. Images were obtained using a T1-weighted 3D spoiled gradient echo sequence (TR=8.1 ms, TE=4 ms, flip angle=30°). Fat suppression was not employed. The patients were scanned in prone position using a standard double breast coil on a 1.5 T whole-body MRI system (Siemens Vision, Siemens, Erlangen, Germany). After the acquisition of the precontrast series, Gd-DTPA contrast agent was delivered intravenously by power injection with a dose of 0.2 mmol/kg and a flow rate of 2 ml/s. Injection of contrast was followed by a saline flush of 20 ml with the same flow rate. Five postcontrast series were then taken with a time interval of 60 s. Each series contained 64 coronal slices with a matrix of 128×256 pixels and an in-plane resolution of $1.25 \times 1.25\ \text{mm}^2$. Slice thickness ranged from 2 to 3 mm depending on breast size. The image database had been retrospectively collected under an IRB-approved protocol.

B. Methods

The computerized interpretation scheme used in this study begins with the segmentation of the lesion within the image. The suspect masses were delineated both manually by an experienced radiologist (U.B.) and automatically by the computer using a 3D volume-growing algorithm.[19] Next, multiple features that characterize the spatial and kinetic properties of the lesions, and thus would potentially help differentiate the malignant cases from the benign cases, were extracted automatically. Stepwise feature selection[20] was employed to select a set of features that perform efficiently in classifying the lesions as malignant or benign. Using linear discriminant analysis[21] (LDA), the selected features were then merged into a single numerical value that is related to estimated likelihood of malignancy.

We evaluated the classification performance of individual features and the merged discriminant score in the task of distinguishing between malignant and benign lesions by using receiver operating characteristics (ROC) analysis.[22] The areaunder the maximum likelihood-fitted binormal ROC curve, A_z, was used as an index of performance.[23] We used the CLABROC[24,25] algorithm to determine the statistical significance (p value) of the difference between two A_z values, associated with two lesion delineation methods. The CLABROC algorithm uses a univariate z-score test to test the difference between areas under two ROC curves.

TABLE I. Features investigated in this study are grouped into three major categories.

I. Morphologic
$F_{I,1}$: Maximum std. of RGH value
$F_{I,2}$: Circularity
$F_{I,3}$: Irregularity
$F_{I,4}$: Margin gradient
$F_{I,5}$: Variance of margin gradient
II. Enhancement kinetics
$F_{II,1}$: Maximum uptake
$F_{II,2}$: Peak location
$F_{II,3}$: Uptake rate
$F_{II,4}$: Washout rate
III. Enhancement-variance dynamics
$F_{III,1}$: Maximum enhancement-variance
$F_{III,2}$: Peak location
$F_{III,3}$: Increasing rate
$F_{III,4}$: Decreasing rate
$F_{III,5}$: Enhancement-variance at time #1

1. Lesion delineation

For the manual delineation, a radiologist (U.B.), blinded to the histological diagnosis, contoured the enhanced tumor area in each slice that intersected the lesion in the subtraction images (postcontrast minus precontrast), using the nonsubtracted MR images as reference.

For the automatic segmentation by computer, we used a volume-growing based algorithm.[19] In this algorithm, the breast volume is first segmented at a threshold derived from the global histogram of voxel-values by maximizing the interclass variance between breast and background. Then the border of the segmented breast volume is removed by morphological erosion using a $3 \times 3 \times 3$ structuring element. Next, regions with high contrast uptake are enhanced by voxelwise computation of the variance of the voxel values over time. A spherical region of interest (SROI) that encompasses the enhanced region is then automatically selected from a set of spheres expanding outwards from a manually selected seed point. From the preprocessed volume within the SROI, a segmentation threshold is then computed by maximizing the interclass variance between enhanced lesion and background voxels in the SROI. Finally, 6-point-connected volume growing is performed to yield the 3D segmented lesion.

2. Computerized feature extraction

In this study, our primary interest is to investigate the potential of enhancement variance dynamics features in the classification of suspicious lesions as malignant or benign. Other features are studied as well for comparison. Features investigated in this study, as listed in Table I, are grouped into three categories: (I) morphological features, (II) enhancement kinetics based features, and (III) features related to the time course of enhancement-variance over the lesion.

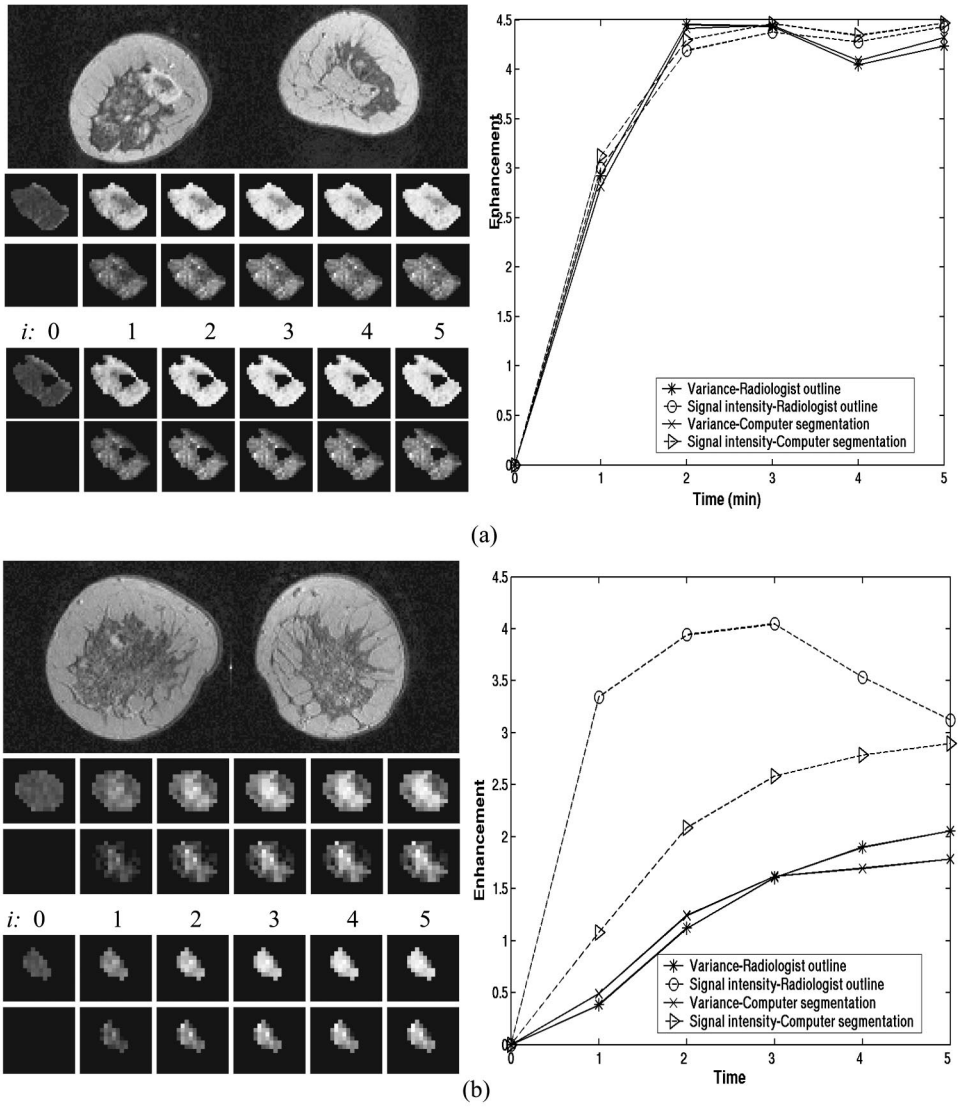

FIG. 1. Examples of lesion segmentation and the corresponding enhancement kinetics and enhancement-variance dynamics curves: (a) malignant case and (b) benign case. In each case, a central slice image of the volume lesion is shown (upper left). Also shown are the radiologist-outlined lesions and the corresponding lesion enhancement [Eq. (1)] at six time points (middle left), the computer-segmented lesion, and the corresponding lesion enhancement at six time points (lower left). The associated kinetics curves are shown (right).

The features in the first category have been described in detail in a previous paper from our group[12] and are only summarized here.

(i) Morphological features.[12] The feature "**maximum standard deviation (std) of radial gradient histogram (RGH)**" ($F_{I,1}$) quantifies how well the image structures in a suspected lesion extend in a spherical pattern originating from the center of the lesion. The feature "**circularity**" ($F_{I,2}$) measures conformity of a lesion to a spherical shape and the feature "**irregularity**" ($F_{I,3}$) indicates the roughness of the lesion surface. The features "**margin gradient**" ($F_{I,4}$) and "**variance of margin gradient**" ($F_{I,5}$) are related to the sharpness of the lesion margin by evaluating voxel-value gradients and their variations along the margin of the suspect lesion.

(ii) Enhancement kinetics based features. Enhancement kinetics is related to the time course of signal intensity within the lesion. Denote $S(\mathbf{r},i)$ as the voxel value at location $\mathbf{r}$ in the lesion at time frame i, i runs from 0 (i.e., the precontrast frame) to 5 (i.e., the last postcontrast frame). For each voxel in the lesion, the contrast enhancement is computed:

$$C(\mathbf{r},i)=\frac{S(\mathbf{r},i)-S(\mathbf{r},0)}{S(\mathbf{r},0)}, \quad i=0,1,...,5. \tag{1}$$

$C(\mathbf{r},i)$ is a quantity that has been shown[26] to be related to Gd-DTPA concentration in the extracellular space of breast tissue at voxel $\mathbf{r}$. In special circumstances this relation approaches linearity. Note that at $i=0, C(\mathbf{r},i)=0$. The enhancement dynamics can be described by the average enhancement over the lesion at each time point, i.e.,

$$\overline{C}(i)=\frac{1}{L}\sum_{r=1}^{L} C(\mathbf{r},i), \quad i=0,1,...,5, \tag{2}$$

where L is the number of voxels in the segmented lesion.

Four features are derived from the enhancement kinetics. The **maximum uptake** ($F_{II,1}$) is the maximum enhance-

ment, i.e., $F_{II,1}=\max_{i=0,1...,5}\overline{C}(i)$. The time frame index at which the maximum enhancement occurs is a feature and is referred to here as "**peak location**" ($F_{II,2}$).

The **uptake rate** ($F_{II,3}$) of the contrast agent is defined as

$$F_{II,3}=F_{II,1}/F_{II,2}. \tag{3}$$

The **washout rate** ($F_{II,4}$) of the contrast agent is defined as

$$F_{II,4}=\begin{cases}\dfrac{F_{II,1}-\overline{C}(5)}{5-F_{II,2}} & (F_{II,2}\neq 5),\\ 0 & (F_{II,2}=5).\end{cases} \tag{4}$$

(iii) Enhancement-variance dynamics features. Enhancement-variance dynamics describes the time course of the spatial variance of the enhancement within the lesion and is defined by

$$V(i)=\frac{1}{L-1}\sum_{r=1}^{L}[C(\mathbf{r},i)-\overline{C}(i)]^2, \quad i=0,1,...,5. \tag{5}$$

Five features are derived from the enhancement-variance dynamics. The **maximum variation of enhancement** ($F_{III,1}$) is the maximum spatial variance of enhancement, i.e., $F_{III,1}=\max_{i=0,1...,5}V(i)$. The time frame index at which the maximum variance occurs is a feature and is referred to here as "**peak location**" ($F_{III,2}$) of the enhancement-variance dynamics.

The **enhancement-variance increasing rate** ($F_{III,3}$) describes how fast the enhancement-variation within the lesion reaches maximum, defined by

$$F_{III,3}=F_{III,1}/F_{III,2}. \tag{6}$$

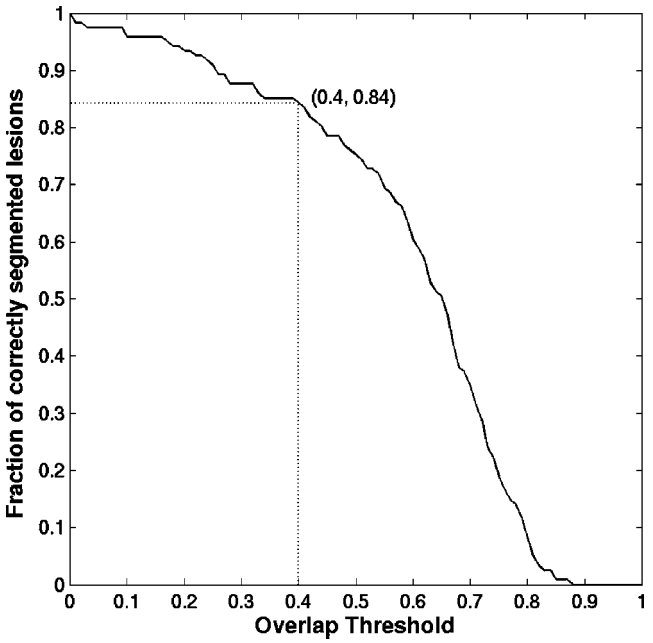

FIG. 2. Performance of the computer segmentation as compared to radiologist segmentation. Curve indicates the fraction of lesions correctly segmented as a function of the overlap criterion.

The **enhancement-variance decreasing rate** ($F_{III,4}$) indicates how fast the enhancement-variance decreases from the maximum, defined by

$$F_{III,4}=\begin{cases}\dfrac{F_{III,1}-V(5)}{5-F_{III,2}} & (F_{III,2}\neq 5),\\ 0 & (F_{III,2}=5).\end{cases} \tag{7}$$

TABLE II. Performance of 14 computer-extracted features in distinguishing between malignant and benign breast lesions that are delineated by both radiologist (column 2) and computer (column 3). The value after "±" is the standard deviation (s.d.) associated with each A_z value. The two tailed p-value was calculated using the univariate z-score test.

Feature	$A_z\pm 1$ s.d.: Radiologist outlined	$A_z\pm 1$ s.d: Computer segmented	p-value
I. Morphologic			
$F_{I,1}$: Maximum std. of RGH value	0.59±0.05	0.56±0.05	0.33
$F_{I,2}$: Circularity	0.57±0.06	0.65±0.05	0.42
$F_{I,3}$: Irregularity	0.66±0.05	0.54±0.06	0.19
$F_{I,4}$: Margin gradient	0.58±0.06	0.60±0.06	0.57
$F_{I,5}$: Variance of margin gradient	0.60±0.05	0.51±0.06	0.03
II. Enhancement kinetics			
$F_{II,1}$: Maximum uptake	0.55±0.06	0.51±0.06	0.25
$F_{II,2}$: Peak location	0.75±0.05	0.79±0.05	0.15
$F_{II,3}$: Uptake rate	0.68±0.05	0.66±0.05	0.50
$F_{II,4}$: Washout rate	0.73±0.05	0.78±0.05	0.09
III. Enhancement-variance dynamics			
$F_{III,1}$: Maximum variation of enhancement	0.50±0.06	0.52±0.06	0.86
$F_{III,2}$: Peak location	0.74±0.05	0.77±0.05	0.08
$F_{III,3}$: Increasing rate	0.58±0.06	0.58±0.06	0.96
$F_{III,4}$: Decreasing rate	0.74±0.05	0.73±0.05	0.90
$F_{III,5}$: Enhancement-variance at time #1	0.65±0.06	0.63±0.06	0.31

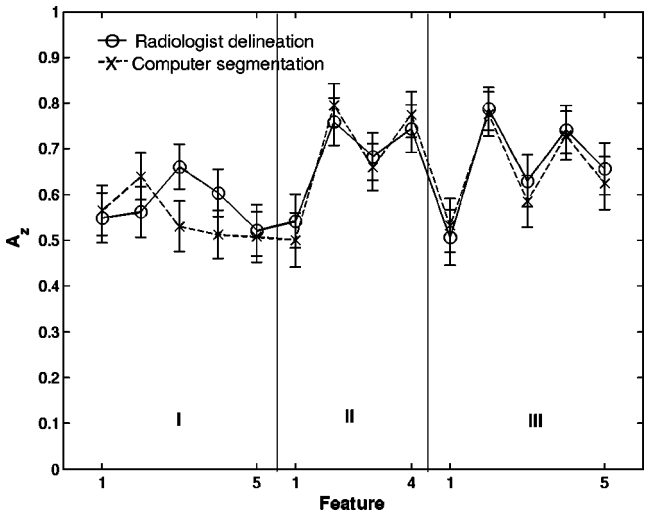

FIG. 3. Performance of the 14 computer-extracted features in distinguishing between malignant and benign breast lesions that are delineated by both radiologist (solid) and computer (dash).

The **enhancement-variance at the first postcontrast frame** ($F_{III,5}$), $V(1)$, reveals the uptake inhomogeneity at the early phase of uptake.

Figure 1 shows two examples (one malignant and one benign) of lesion segmentation and the corresponding enhancement kinetics curves and enhancement-variance curves. Note that the lesion sizes in the two examples are different, so in the figure the pixels of the smaller lesion [Fig. 1(b)] look larger.

III. RESULTS

Performance of the computer segmentation is shown in Fig. 2. Here overlap is defined as the volume of intersection of the radiologist-delineated lesion and the computer-segmented lesion divided by the volume of their union. In this database with 121 mass lesions, 84% of the lesions were correctly segmented at an overlap threshold of 0.4. The two segmentation examples shown in Fig. 1 had overlaps of (a) 0.77 and (b) 0.17, respectively.

Table II and Fig. 3 show the A_z values and the associated standard deviations indicating individual performance levels of the 14 features in the task of distinguishing between malignant and benign breast lesions that were delineated by either radiologist or computer. The results indicate that all three categories of features show potential for the classification task.

As also demonstrated in Table II and Fig. 3, at the significance level $p=0.05$, we failed to show a statistically significant difference between the performance (i.e., A_z) of features obtained using the radiologist-outlined lesions and the performance of those obtained with the computer-segmentation (except for feature $F_{I,5}$) in the task of distinguishing between malignant and benign breast lesions.

Stepwise feature selection[20] selected two sets of features—one set for each of the two methods of lesion delineation (Table III). The selected feature-set from features based on the radiologist-outlined lesions (set 1) includes four features: peak location of enhancement-variance dynamics ($F_{III,2}$), irregularity ($F_{I,3}$), washout rate of enhancement kinetics ($F_{II,4}$), and peak location of enhancement kinetics ($F_{II,2}$). The leave-one-out cross-validation using linear discriminant analysis to merge the selected features yields an A_z value of 0.80 in the task of distinguishing between malignant and benign lesions. The selected feature-set from features based on the computer-segmented lesions (set 2) includes six features: peak location of enhancement-variance dynamics ($F_{III,2}$), enhancement-variance increasing rate ($F_{III,3}$), peak location of enhancement kinetics ($F_{II,2}$), margin gradient ($F_{I,4}$), variance of margin gradient ($F_{I,5}$), and maximum standard deviation of RGH value ($F_{I,1}$). The leave-one-out cross-validation using linear discriminant analysis to merge the selected features yields an A_z value of 0.86.

IV. DISCUSSION

Enhancement kinetic analysis evaluates how the contrast enhancement within the lesion changes in a period of time, and reveals the uptake and washout characteristics of the intravenous contrast within a lesion. Studies have shown that malignant cases tend to have rapid uptake and washout.[12] Our results are consistent with such published results. In our analysis, 64% of the benign lesions showed no washout over the six acquisition frames, i.e., their enhancement-curves keep increasing. For malignant lesions only 24% demonstrated no washout. It is worth noting that all the features are calculated based on the average enhancement of the entire lesion. In clinical practice, however, radiologists can choose any region with which to assess the enhancement kinetics. Our future work of interest is to develop automatic methods to extract region of maximum enhancement. The enhancement-kinetics based features on such ''hot areas'' are expected to perform better in differential diagnosis.

Enhancement-variance dynamics reveals how the spatial distribution of contrast enhancement in the lesion region changes in a period of time. Our results showed that the spatial variance of enhancement peaks earlier in malignant lesions (Fig. 4). The enhancement-variance in a particular

TABLE III. Stepwise feature selection and the performance of the merged features using leave-one-out cross-validation. The value after ''±'' is the standard deviation (s.d.) associated with each A_z value. The two-tailed p-value was calculated using the univariate z-score test.

Radiologist outlined lesions		Computer segmented lesions		
Feature Set 1	$A_z \pm 1$ s.d.	Feature Set 2	$A_z \pm 1$ s.d.	p-value
$F_{III,2}F_{I,3}F_{II,4}F_{II,2}$	0.80 ± 0.04	$F_{III,2}F_{III,3}F_{II,2}F_{I,4}F_{I,5}F_{I,1}$	0.86 ± 0.04	0.07

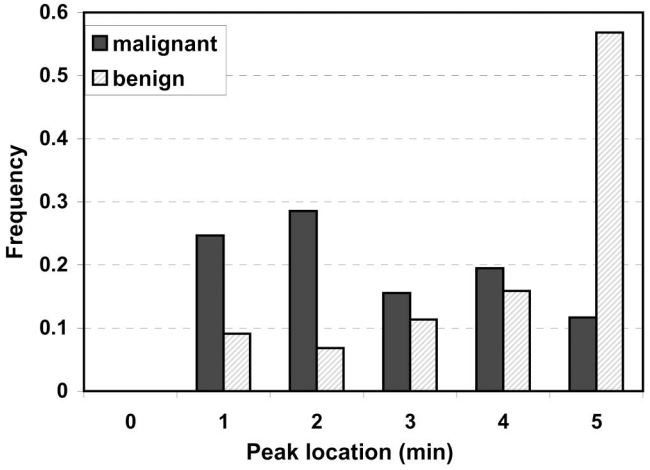

FIG. 4. Histogram of peak location of enhancement-variance dynamics for the computer-segmented lesions.

time frame reveals the degree of inhomogeneity of the enhancement. Our results show that malignant lesions tend to be less homogenous at the first postcontrast time frame ($F_{III,5}$). However, malignant and benign lesions showed similar results for the maximum inhomogeneity ($F_{III,1}$), as determined over all time frames.

The relative performance of the morphological and kinetic features depends on the MR imaging protocol involved. Basically, morphologic features perform better in high spatial resolution images and enhancement kinetics features perform better in high temporal resolution images.[27] Intuitively, morphological features might be more sensitive to lesion delineation methods. With the imaging protocol and lesion segmentation methods used in this study, overall, the kinetics features appeared to perform better than did the morphological features in the task of distinguishing between malignant and benign lesions.

At present, protocols used in breast MR imaging worldwide are far from reaching a consensus and optimal imaging parameters are still under investigation. The imaging technique used in our study is similar to that launched by Kaiser *et al.*,[2] which was called "the archetype of dynamic breast MRI" by Kuhl *et al.*:[5] acquisition of one precontrast and a series of postcontrast images including both breasts at a temporal resolution of 60 s. A potential limitation of the technique is that the data were acquired over only 5 min after contrast injection, as there is probably some useful information beyond 5 min.[28] The choice of the parameters is a tradeoff to allow for a shorter exam time, which is better accepted by patients and is less costly. This limited acquisition time problem might have some influence on the performance of washout related features ($F_{II,4}$,$F_{II,4}$). The influence on the performance of other temporal features should be much less severe as, in most cases, the signal reaches plateau within 5 min. We regard as an interesting research question the effect of acquisition time on the performance of computer-extracted features in distinguishing between malignant and benign lesions.

V. CONCLUSION

Our investigation with automated feature extraction and classification indicates that spatial-variance dynamics is a promising family of features in the task of distinguishing between malignant and benign MR breast lesions. Combining the morphological features of contrast enhancements, enhancement kinetics features, and the enhancement-variance dynamics features using computerized methods has the potential to complement the interpretation of radiologists in a consistent, objective, and accurate way.

ACKNOWLEDGMENTS

The research was supported in part by USPHS Grant No. CA89452 and DOD Breast Cancer Research Program DAMD 17-03-1-0245. MLG, LL, and UB are shareholders in R2 Technology, Sunnyvale, CA. It is the policy of the University of Chicago that investigators disclose publicly actual or potential significant financial interests that may appear to be affected by the research activities.

[a)]Presented in part at the 2002 annual meeting of the AAPM, Montreal, Canada and the 2002 annual meeting of the RSNA, Chicago, IL.

[b)]Author to whom correspondence should be addressed. Electronic mail: m-giger@uchicago.edu

[1] S. H. Heywang, D. Hahn, H. Schmidt, I. Krischke, W. Eiermann, R. Bassermann, and J. Lissner, "MR imaging of the breast using gadolinium-DTPA," J. Comput. Assist. Tomogr. **10**, 199–204 (1986).

[2] W. A. Kaiser and E. Zeitler, "MR imaging of the breast: fast imaging sequence with and without Gd-DTPA," Radiology **170**, 681–686 (1989).

[3] S. H. Heywang, A. Wolf, E. Pruss, T. Hilbertz, W. Eiermann, and W. Permanetter, "MR imaging of the breast with Gd-DTPA: use and limitations," Radiology **171**, 95–103 (1989).

[4] S. G. Orel and M. D. Schnall, "MR imaging of the breast for the detection, diagnosis, and staging of breast cancer," Radiology **220**, 13–30 (2001).

[5] C. K. Kuhl and H. H. Schild, "Dynamic image interpretation of MRI of the breast," J. Magn. Reson Imaging **12**, 965–974 (2000).

[6] D. M. Ikeda, N. M. Hylton, K. Kinkel, M. G. Hochman, C. K. Kuhl, W. A. Kaiser, J. C. Weinreb, S. F. Smazal, H. Degani, P. Viehweg, J. Barclay, and M. D. Schnall, "Development, standardization, and testing of a lexicon for reporting contrast-enhanced breast magnetic resonance imaging studies," J. Magn. Reson Imaging **13**, 889–895 (2001).

[7] S. G. Orel, M. D. Schnall, and C. M. Powell, "Staging of suspected breast cancer: effect of MR imaging and MR guided biopsy," Radiology **196**, 115–122 (1995).

[8] L. W. Nunes, M. D. Schnall, S. G. Orel, M. G. Hochman, C. P. Langlotz, C. A. Reynolds, and M. H. Torosian, "Breast MR imaging: interpretation model," Radiology **202**, 833–841 (1997).

[9] L. W. Nunes, M. D. Schnall, and S. G. Orel, "Update of breast MR imaging architectural interpretation model," Radiology **219**, 484–494 (2001).

[10] P. F. Liu, J. F. Debatin, R. F. Caduff, G. Kacl, E. Garzoli, and G. P. Krestin, "Improved diagnostic accuracy in dynamic contrast enhanced MRI of the breast by combined quantitative and qualitative analysis," Br. J. Radiol. **71**, 501–509 (1998).

[11] A. J. Bradley, B. M. Carrington, C. L. Hammond, R. Swindell, and B. Magee, "Accuracy of axillary MR imaging in treated breast cancer for distinguishing between recurrent tumor and treatment effects: does intravenous Gd-DTPA enhancement help in cases of diagnostic dilemma," Clin. Radiol. **55**, 921–928 (2000).

[12] C. K. Kuhl, P. Mielcareck, S. Klaschik, C. Leutner, E. Wardelmann, J. Gieseke, and H. H. Schild, "Dynamic breast MR imaging: Are signal intensity time course data useful for differential diagnosis of enhancing lesion?," Radiology **211**, 101–110 (1999).

[13] K. G. A. Gilhuijs, M. L. Giger, and U. Bick, "Computerized analysis of breast lesions in three dimensions using dynamic magnetic-resonance imaging," Med. Phys. **25**, 1647–1654 (1998).

[14] E. A. Morris, ''Breast cancer imaging with MRI,'' Radiol. Clin. North Am. **40**, 443–466 (2002).
[15] P. J. Kneeshaw, L. W. Turnbull, and P. J. Drew, ''Current applications and future direction of MR mammography,'' Br. J. Cancer **88**, 4–10 (2003).
[16] K. Kinkel, T. H. Helbich, L. J. Esserman, J. Barclay, E. H. Schwerin, E. A. Sickles, and N. M. Hylton, ''Dynamic high-spatial-resolution MR imaging of suspicious breast lesions: Disgnostic criteria and interobserver variability,'' AJR, Am. J. Roentgenol. **175**, 35–43 (2000).
[17] S. J. Kim, E. A. Morris, L. Liberman, D. J. Ballon, L. R. L. Trenta, O. Hadar, A. Abramson, and D. D. Dershaw, ''Observer variability and applicability of BI-RADS terminology for breast MR imaging: Invasive carcinomas as focal masses,'' AJR, Am. J. Roentgenol. **177**, 551–557 (2001).
[18] U. Wedegärtner, U. Bick, K. Wörtler, E. Rummeny, and G. Bongartz, ''Differentiation between benign and malignant findings on MR-mammography: usefulness of morphological criteria,'' Eur. Radiol. **11**, 1645–1650 (2001).
[19] K. G. A. Gihuijs, M. L. Giger, and U. Bick, ''A method for computerized assessment of tumor extent in contrast-enhanced MR images of the breast,'' in *Computer-Aided Diagnosis in Medical Imaging*, edited by K. Doi, H. MacMahon, M. L. Giger, and K. R. Hoffmann (Elsevier, Amsterdam, 1999), pp. 305–310.
[20] J. Neter, W. Wasserman, and M. H. Kutner, *Applied Linear Statistical Models Regression, Analysis of Variance, and Experimental Designs*, 2nd ed. (Irwin, Homewood, 1985).
[21] R. A. Johnson and D. W. Wichern, *Applied Multivariate Statistical Analysis*, 3rd ed. (Prentice–Hall, Englewood Cliffs, NJ, 1992).
[22] C. E. Metz, ''Some practical issues of experimental design and data analysis in radiological ROC studies,'' Invest. Radiol. **24**, 234–245 (1989).
[23] Y. Jiang, C. E. Metz, and R. M. Nishikawa, ''A receiver operating characteristic partial area index for highly sensitive diagnostic tests,'' Radiology **201**, 745–750 (1996).
[24] C. E. Metz, P-L. Wang, and H. B. Kronman, ''A new approach for testing the significance of differences between ROC curves measured from correlated data,'' in *Information Processing in Medical Imaging*, edited by Deconinck (Nijhoff, The Hague, The Netherlands, 1984), pp. 432–435.
[25] C. E. Metz, B. A. Herman, and C. A. Roe, ''Statistical comparison of two ROC-curve estimates obtained from partially-paired datasets,'' Med. Decision Making **18**, 110–121 (1998).
[26] U. Hoffmann, G. Brix, M. V. Knopp, T. Heb, and W. J. Lorenz, ''Pharmacokinetic mapping of the breast: A new method for dynamic MR mammography,'' Magn. Reson. Med. **33**, 506–514 (1995).
[27] J. C. Weinreb and G. Newstead, ''MR imaging of the breast,'' Radiology **196**, 593–610 (1995).
[28] H. Sherif, A. E. Mahfouz, H. Oellinger, J. Hadijuana, J. U. Blohmer, M. Taupitz, R. Felix, and B. Hamm, ''Peripheral washout sign on contrast-enhanced MR images of the breast,'' Radiology **205**, 209–213 (1997).

A Fuzzy C-Means (FCM)-Based Approach for Computerized Segmentation of Breast Lesions in Dynamic Contrast-Enhanced MR Images[1]

Weijie Chen, MSc, Maryellen L. Giger, PhD, Ulrich Bick, MD

Rationale and Objectives. Accurate quantification of the shape and extent of breast tumors has a vital role in nearly all applications of breast magnetic resonance (MR) imaging (MRI). Specifically, tumor segmentation is a key component in the computerized assessment of likelihood of malignancy. However, manual delineation of lesions in four-dimensional MR images is labor intensive and subject to interobserver and intraobserver variations. We developed a computerized lesion segmentation method that has the advantage of being automatic, efficient, and objective.

Materials and Methods. We present a fuzzy c-means (FCM) clustering-based method for the segmentation of breast lesions in three dimensions from contrast-enhanced MR images. The proposed lesion segmentation algorithm consists of six consecutive stages: region of interest (ROI) selection by a human operator, lesion enhancement within the selected ROI, application of FCM on the enhanced ROI, binarization of the lesion membership map, connected-component labeling and object selection, and hole-filling on the selected object. We applied the algorithm to a clinical MR database consisting of 121 primary mass lesions. Manual segmentation of the lesions by an expert MR radiologist served as a reference in the evaluation of the computerized segmentation method. We also compared the proposed algorithm with a previously developed volume-growing (VG) method.

Results. For the 121 mass lesions in our database, 97% of lesions were segmented correctly by means of the proposed FCM-based method at an overlap threshold of 0.4, whereas 84% of lesions were correctly segmented by means of the VG method.

Conclusion. Our proposed algorithm for breast-lesion segmentation in dynamic contrast-enhanced MRI was shown to be effective and efficient.

Key Words. Tumor segmentation; dynamic contrast-enhanced magnetic resonance imaging; fuzzy c-means; computer-aided diagnosis; breast cancer.

Breast cancer is the most common cancer and the second leading cause of cancer death in women in Western countries. Imaging has a crucial role in the workup of patients with breast cancer, with contributions to early detection through screening, diagnosis and associated image-guided biopsy, treatment planning, and treatment response monitoring. X-Ray mammography has shown considerable success in screening for the early detection of breast cancer; however, some limitations exist, such as low specificity leading to unnecessary biopsies, presentation of cancer lesions as radiographically occult in dense breasts, and the inherent limitations of two-dimensional (2D) projection image data. Thus, extensive efforts in the past 15 years have included the use of magnetic resonance (MR) imaging (MRI) and sonography as complementary imaging modalities to improve breast-imaging interpretation (1).

Acad Radiol 2006; 13:63–72

[1] From the University of Chicago, Radiology, 584 South Maryland, MC Chicago, IL 60637 (W.C.), Charite University Medicine, Department of Radiology, Campus Mitte, Berlin, Germany. Received July 25, 2005; Revision received August 25; Revision accepted August 27. Supported in part by Breast Cancer Research Program grant no. DAMD17-03-1-0245 from the Department of Defense and grant no. CA89452 from the US Public Health Service. M.L.G. is a shareholder in R2 Technology, Sunnyvale, CA. It is the policy of the University of Chicago that investigators disclose publicly actual or potential significant financial interests that may appear to be affected by the research activities. **Address correspondence to:** W.C. e-mail: weijie@uchicago.edu

doi:10.1016/j.acra.2005.08.035

Dynamic contrast-enhanced MRI (DCE-MRI) using gadopentate dimeglumine (Gd-DTPA) as contrast agent has gained much recognition in breast imaging since the findings of Heywang et al (2,3) and Kaiser and Zeitler (4). In a typical dynamic study, three-dimensional (3D) images of both breasts are acquired before and repeatedly after injection of the contrast agent Gd-DTPA. In postcontrast serial images, MR signal intensity over cancerous lesion areas is enhanced because of increased vascularity of tumors. Contrast-enhanced MR images of the breast provide 3D spatial information about the lesions and temporal information about lesion physiology, allowing for more accurate assessment of lesion extent and better lesion characterization. In recent years, breast MRI has become more widely used for difficult diagnostic evaluations, monitoring chemotherapy response, and evaluation of disease extent (1,5).

Accurate quantification of the shape and extent of breast tumors has a vital role in nearly all applications of breast MRI. Specifically, tumor segmentation is a key component in computerized assessment of the likelihood of malignancy (6,7). MRI has yielded higher correlation between measured tumor size and actual tumor size than mammography and sonography (8–10). In current clinical settings, MR images typically are examined visually by radiologists on a slice-by-slice basis. However, visual assessment of lesion extent in three dimensions from 2D slices may be difficult, especially in irregular masses. For example, in a typical dynamic MR study, six time series may be acquired, each containing 60 slices; thus, manual delineation of lesion margins becomes labor intensive. In addition, random variations up to 29% have been reported between true and observed tumor size by using manual delineation on MRI (8). These variations may be caused in part by interobserver and intraobserver differences in analyses.

Computerized techniques may improve the objectivity, consistency, and efficiency of the segmentation of breast lesions, as shown in other areas, such as mammography (11,12) and sonography (13,14). For lesion segmentation in breast MR images, Lucas-Quesada et al (15) proposed semiautomated methods based on 2D slice-by-slice analysis of MR images. Gihuijs et al (16) developed a 3D lesion segmentation method in which volume growing (VG) was performed from a user-specified seed point. In previous studies (6,7), we investigated computerized methods for assessing the likelihood of malignancy of suspicious masses, based on both delineation of the lesion by a radiologist and segmentation of the lesion with the VG method (16).

In this study, we present a novel 3D lesion segmentation method based on the fuzzy c-means (FCM) clustering algorithm. We evaluate our method by comparing computerized segmentation against radiologists' outlines on a clinical database of mass lesions. We also compare the proposed algorithm with our previously developed VG approach (16).

MATERIALS AND METHODS

Database

The image database in this study was collected retrospectively under an institutional review board–approved protocol. Images were obtained by using a T1-weighted 3D spoiled gradient echo sequence (repetition time = 8.1 milliseconds, echo time = 4 milliseconds, flip angle = 30°). Patients were scanned while in the prone position by using a standard double-breast coil on a 1.5-Tesla whole-body MRI system (Siemens Vision; Siemens, Erlangen, Germany). After acquisition of the precontrast series, Gd-DTPA contrast agent was delivered intravenously by power injection with a dose of 0.2 mmol/kg and flow rate of 2 mL/s. Injection of contrast was followed by a 20-mL saline flush with the same flow rate. Five postcontrast series were obtained, with an interval of 69 seconds. Each series contained 64 coronal slices with a matrix of 128 × 256 pixels and in-plane resolution of 1.25 × 1.25 mm. Slice thickness ranged from 2.0 to 3.0 mm, depending on breast size.

Our database consists of 121 primary mass lesions from 121 patients, in which 77 lesions are malignant and 44 lesions are benign, confirmed by biopsy. Lesion size varies from 0.02 to 94 cm^3. Distribution of lesions based on manually-delineated tumor size is shown in Figure 1.

Review of FCM Algorithm

FCM is an unsupervised learning technique in the pattern-recognition field (17,18). The goal of FCM is to find the (fuzzy) partition of data set X comprising N data points ($X = \{\mathbf{x}_i, i = 1,2,\ldots,N | \mathbf{x}_i \in \Re^m\}$) into c classes (aka "clusters," "groups"). The data point x_i is an m-dimensional feature vector. The (unknown) class prototypes are represented by a c by m matrix V, the k^{th} ($k = 1, 2, \ldots, c$) row, which is an m-dimensional vector and represents the prototype of the k^{th} class. The partition is represented by a c by N *partition matrix* U. The element of matrix U, u_{ki},

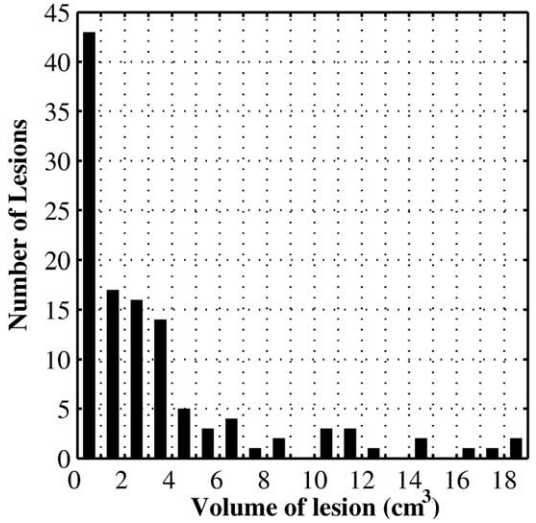

Figure 1. Distribution of lesions in our database based on tumor size, delineated by a radiologist.

represents the membership of the i^{th} data point to the k^{th} class. Note that in a crisp partition of data points, the membership value is binary, ie, a data point is assigned a value of 1 if it belongs to the k^{th} class, and 0 otherwise. However, with a fuzzy partition, the membership value (ie, u_{ki}) continuously ranges from 0 to 1 and characterizes the degree of similarity between the i^{th} data point and k^{th} class prototype.

The matrix U is found by minimizing the generalized least squares within-group square error function J_m:

$$J_m = \sum_{k=1}^{c} \sum_{i=1}^{N} u_{ki}^{b} \|\mathbf{x}_i - \mathbf{v}_k\|^2 \quad (1)$$

with the following constraints:

$$\sum_{k=1}^{c} u_{ki} = 1,\ \forall\, i; 0 \le u_{ki} \le 1,\ \forall\, k, i; \sum_{i=1}^{N} u_{ki} > 0,\ \forall\, k \quad (2)$$

where $b \in [1,\infty)$ is a weighting exponent on each fuzzy membership, and $\|\ \|$ denotes the Euclidean distance. The necessary conditions for the within-group square error function to be minimized with the constraints in equation 2 can be derived by LaGrange multipliers:

$$u_{ki} = \frac{1}{\sum_{l=1}^{c} \left(\frac{\|\mathbf{x}_i - \mathbf{v}_k\|}{\|\mathbf{x}_i - \mathbf{v}_l\|} \right)^{2/(b-1)}}, \quad k = 1, 2, \ldots, c;\ i = 1, 2, \ldots, N \quad (3)$$

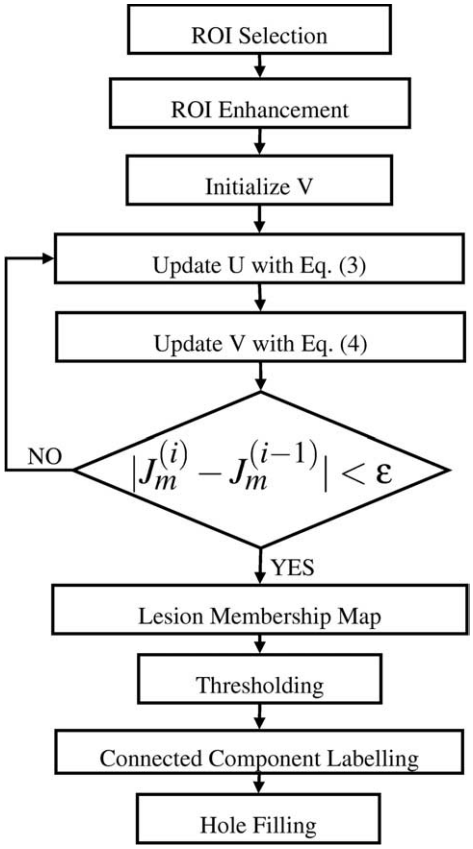

Figure 2. Diagram for the proposed FCM-based lesion segmentation algorithm.

$$v_k = \frac{\sum_{i=1}^{N} u_{ki}^{b} \mathbf{x}_i}{\sum_{i=1}^{N} u_{ki}^{b}}, k = 1, 2, \ldots, c \quad (4)$$

In implementation, matrix V is randomly initialized, and then U and V are obtained through an iterative process using equations 3 and 4. FCM and its variants have been widely used in MR image segmentation (19–21) and analysis of functional MRI of the human brain (22,23). In this study, we investigate the use of FCM for segmentation of breast lesions in DCE-MRI data.

Lesion Segmentation

The proposed lesion segmentation in contrast-enhanced MRI consists of six consecutive stages: region of interest (ROI) selection by a human operator, lesion enhancement within the selected ROI, application of FCM on the enhanced ROI, binarization of the lesion membership map, connected-component labeling and object selection, and hole-filling on the selected object. Figure 2 shows the

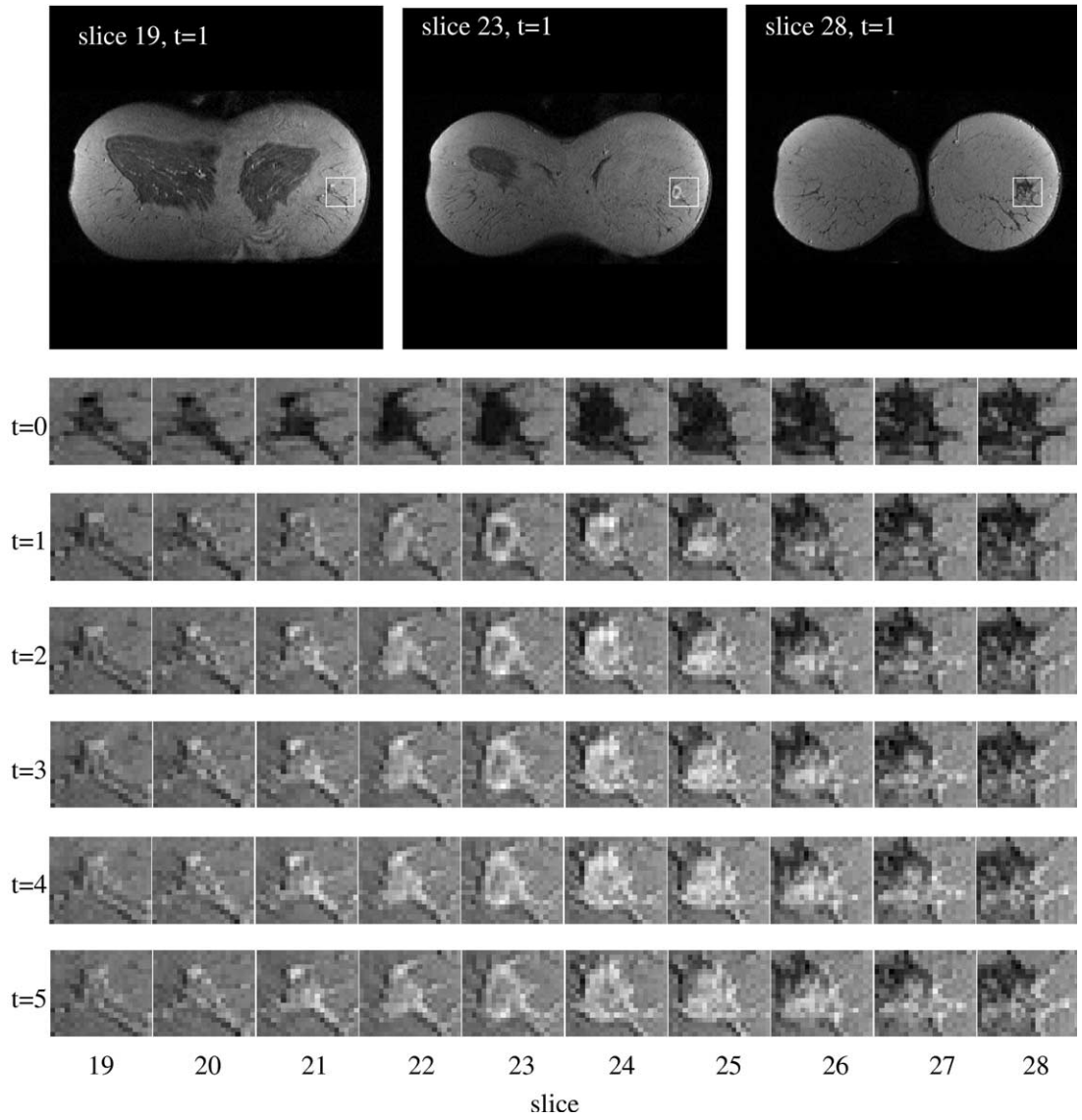

Figure 3. Example of 4D ROI containing a lesion. (Top) Three slices are shown: the first slice, in which the lesion appears; a typical central slice; and the last slice, in which the lesion appears. (Bottom) Time series 3D ROIs in multiple slices, each row representing a time series and each column representing a slice.

diagram of the algorithm. Note that operator interaction is required only at the initial stage to indicate the lesion location. We describe the segmentation strategy in a step-by-step fashion, with an example showing results of each step (Figures 3–6).

As shown in the section Database, volume data in each time series consist of multiple slices. In the first stage, a box-shaped ROI containing the 3D lesion is formed from three inputs of a human operator: (1) first slice in which the lesion appears, (2) last slice in which the lesion appears, and (3) a rectangle bounding the lesion in some representative middle slice. The rectangle defines the largest extent within each slice, and the first slice and the last slice define the cross-slice extent of the lesion. The interaction could be performed quickly with a mouse on a computer's graphical user interface that displays multiple slices simultaneously. Figure 3 (top) shows the first slice, last slice, and a typical central slice that contain the lesion, with a rectangle defining the planar extent of the lesion. Note that only one rectangle is drawn by the human operator, and it then is duplicated on each slice at the same planar location from the first to the last slice. The three slices shown are from the first postcontrast series ($t = 1$). Figure 3 (bottom) shows the four-dimen-

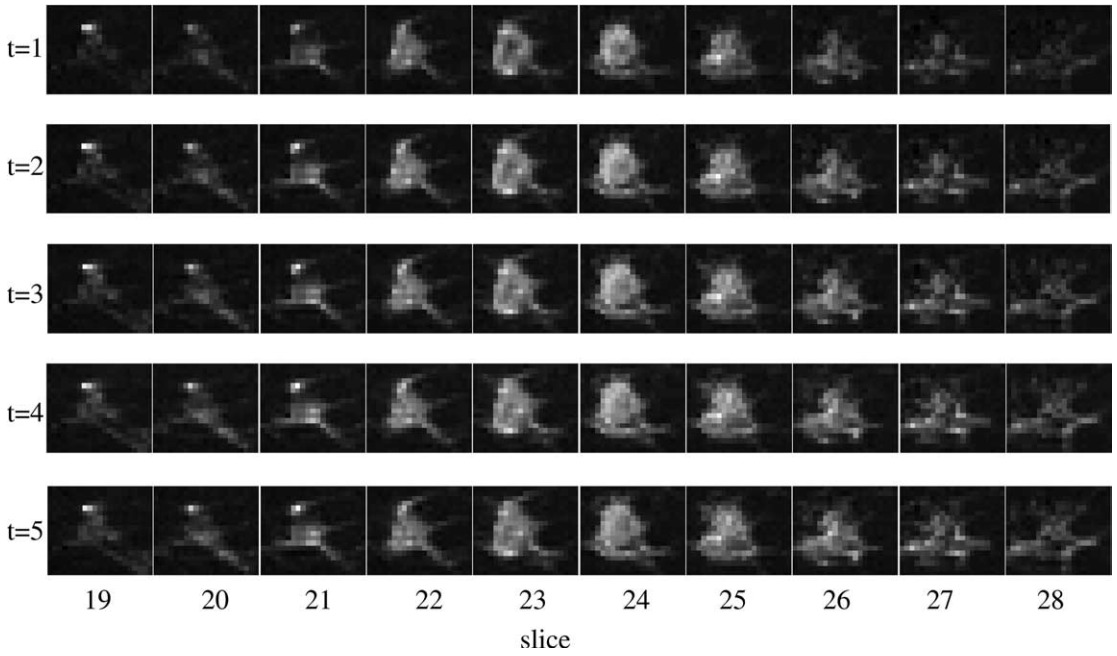

Figure 4. Enhanced postcontrast ROIs: postcontrast ROI series are enhanced by dividing the intensity value at each voxel by the intensity value at the corresponding precontrast voxel.

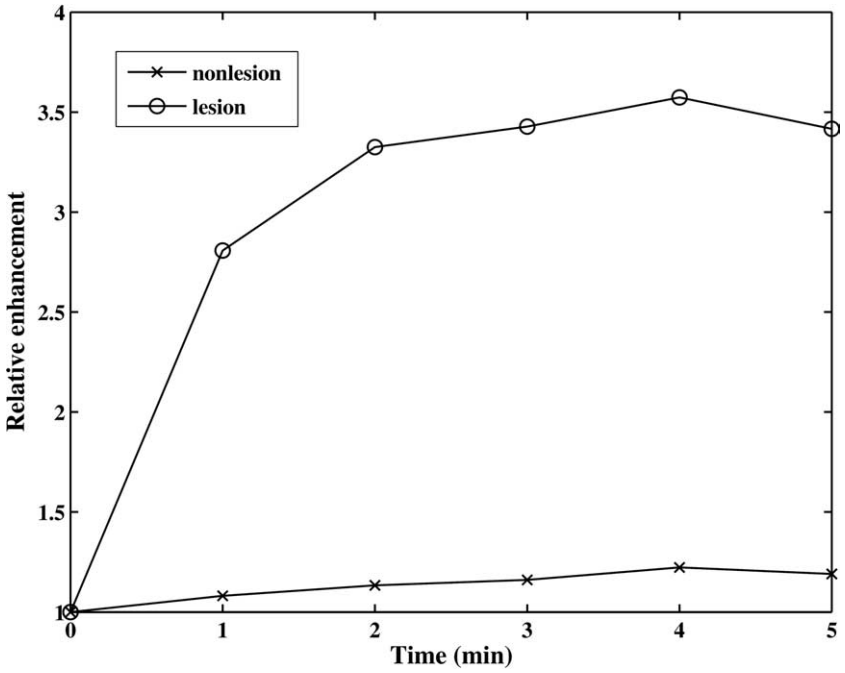

Figure 5. Prototype enhancement curves found by FCM for lesion voxels and nonlesion voxels within the ROI.

sional (4D) ROI, with each row representing a time series and each column representing a slice.

In the second stage, the postcontrast ROI series is enhanced by dividing the intensity value at each voxel by the intensity value at the corresponding precontrast voxel. The enhanced postcontrast ROI series is shown in Figure 4. Given N number of voxels in the ROI, then $x_i(t)$ ($i = 1, 2, \ldots, N$, $t = 1, 2, \ldots, 5$) is the normalized intensity value at voxel i

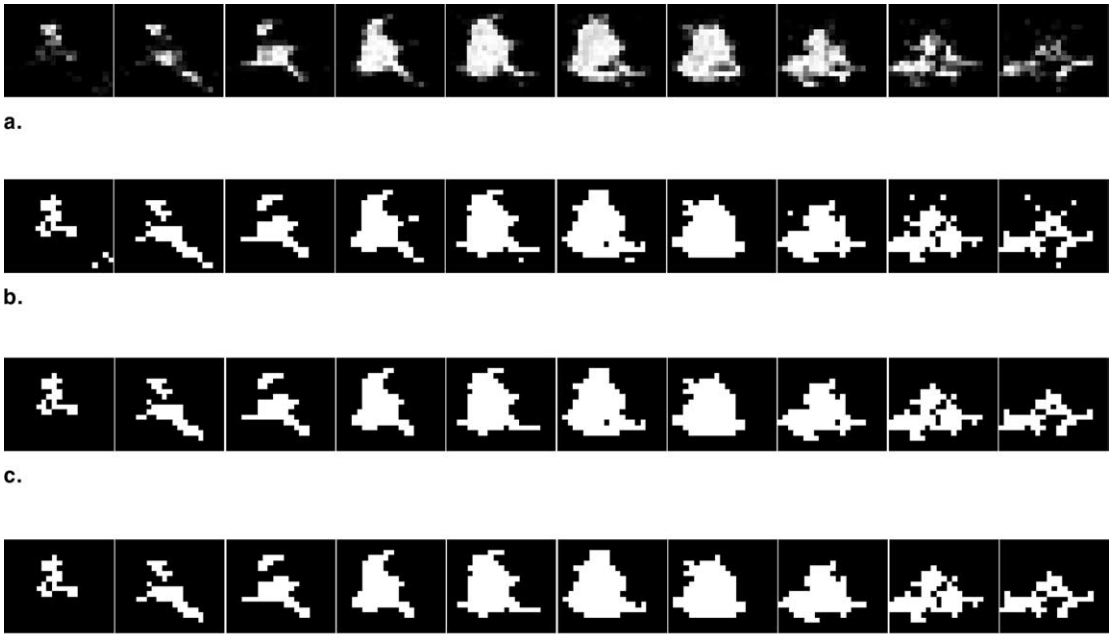

Figure 6. Lesion segmentation using FCM. (a) Lesion membership map from FCM, (b) binarized with a prespecified threshold, (c) connected component labeling and target selection, and (d) hole filling.

of the t^{th} postcontrast series, namely, $x_i(t) = I_i(t)/I_i(0)$, where $I_i(t)$ is the MR intensity value of voxel i at time t.

Next, we apply the FCM algorithm to partition ROI voxels into two categories ($c = 2$): lesion and nonlesion, by using postcontrast-enhanced ROI data, ie, $X = \{\mathbf{x}_i, i = 1,2,\ldots,N | \mathbf{x}_i \in \Re^5\}$. In this application, partition matrix U of size $2 \times N$ and prototype matrix V of size 2×5 are obtained by minimizing the objective function defined in equation 1. Specifically, matrix V is randomly initialized, then U and V are iteratively updated by using equations 3 and 4 until convergence, ie, the absolute change in objective function in consecutive iterations is less than a prespecified small number ϵ ($\epsilon = 10^{-5}$ in this study). The parameter b was set to $b = 2$. Denote the obtained U and V as $U = [U_1\ U_2]^T$ and $V = [V_1\ V_2]^T$, where T denotes matrix transpose and U_k and V_k (k = 1, 2) are row vectors of length N and 5, respectively. The Euclidean norms of V_k (k = 1, 2) are used to determine which row represented the lesion. Denote $l = arg\ \max_k(\|V_k\|)$, then V_l is the prototype enhancement curve of the lesion class, U_l is the lesion membership map because enhancement in the lesion area is much more significant than that in surrounding tissues. The prototype enhancement curves of lesion and nonlesion for the ROI in Figure 3 are shown in Figure 5. The corresponding lesion membership map is shown in Figure 6a.

The lesion membership map then is binarized with an empirically chosen threshold ($TH = 0.2$) (Figure 6b). As shown in Figure 6b, surrounding the lesion, there exist some false-positive voxels that correspond to either vessels or background noise. To reduce these spurious structures, a 3D connected-component labeling operation (24) is performed on the binary ROI by using the following procedure: (1) scan all voxels in the binary ROI and assign preliminary labels to nonzero voxels and record label equivalences; (2) resolve the equivalence classes; and (3) relabel the voxels based on the resolved equivalence classes. After connected-component labeling, the component containing the center of the ROI is selected as the lesion (Figure 6c), and all other labeled components (spurious structures, noise, and so on) are erased (ie, assign zeros to those components). Finally, a hole-filling operation based on morphological resonstruction (25) is performed on the 3D lesion because there might be some necrotic area in the tumor that may have very low enhancement and thus initially is partitioned as nonlesion in the FCM procedure. Figure 6d shows the final segmentation result after hole filling.

Evaluation

In this study, manual segmentation of the lesions by an expert MR radiologist served as reference (ie, the "true

outline") in the evaluation of the computerized segmentation method. Manual segmentation was performed slice by slice in the subtracted images (postcontrast image − precontrast image); the enhanced tumor area in each slice that intersected the lesion was outlined. All subtraction images were used for this purpose, and the radiologist also used the original (nonsubtracted) MR images as additional information. For each delineated lesion, we determined tumor volume by voxel counting.

We also defined an overlap measure as a performance index to quantify agreement between the computerized segmentation and radiologist delineation. For a given lesion, denote C as the set of voxels returned from the computerized segmentation and R as the set of voxels in the radiologist's segmentation. The overlap measure, O, is defined as the intersection of C and R over the union of C and R, ie,

$$O = \frac{C \cap R}{C \cup R} \tag{5}$$

The value of O is bounded between zero (no overlap) and one (exact overlap). Taking the radiologists' delineation as "truth," a lesion is considered to be correctly segmented by the computer when the overlap O between the computerized segmentation and the radiologist's segmentation is larger than a predetermined threshold called overlap threshold.

RESULTS

Figure 7a shows a plot of the fraction of correctly segmented lesions at various overlap threshold levels for both the proposed FCM-based method and our previously reported VG method (16). The proposed method outperformed the VG method, ie, more lesions are segmented correctly by means of FCM than by means of VG at various overlap threshold levels. In particular, 97% of lesions are segmented correctly by means of the proposed FCM-based method at the overlap threshold of 0.4, whereas 84% of lesions are segmented correctly by means of the VG method. Figure 7b shows a plot of the fraction of correct segmentation versus overlap threshold separately for benign and malignant lesions. At the overlap threshold of 0.4, by means of the proposed FCM-based method, 98.7% of malignant lesions and 93.2% of benign lesions are segmented correctly, whereas 93.5% of malignant lesions and 70.5% of benign lesions are segmented correctly by using the VG method.

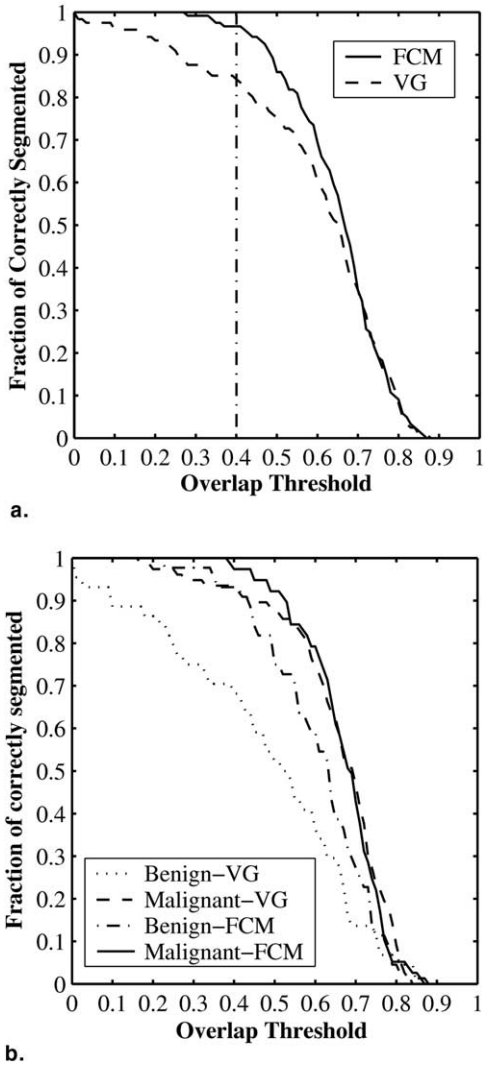

Figure 7. Performance of the proposed FCM-based lesion segmentation algorithm and the previously developed VG algorithm on a clinical database of 121 mass lesions. (a) Evaluated on the entire database and (b) on malignant and benign lesions, respectively.

Table 1 summarizes the statistical comparison of the two methods, FCM and VG, by using the overlap measure and lesion volume. For the 121 mass lesions in our database, FCM yielded an average overlap value of 0.64 with an SD of 0.12, whereas the VG method yielded an average overlap value of 0.59 with an SD of 0.20. The two sets of overlap values of the 121 mass lesions were compared by using paired t-test, and the improvement in overlap values with the proposed method was found to be statistically significant ($P < .002$).

Table 1
Summary of Performance of the Proposed Lesion Segmentation Algorithm

	Overlap			Volume (cm^3)		
Method	Mean ± SD	*P*	Method	Mean ± SD	cc	*P*
FCM	0.64 ± 0.12	<.002	FCM	4.1 ± 8.1	0.98	.71
VG	0.59 ± 0.20		Radiologist	4.7 ± 10.0	0.64	.12
			VG	3.0 ± 4.0		

cc, correlation coefficient between two measurements.
P obtained with paired *t*-test to compare the significance of difference between two measurements.

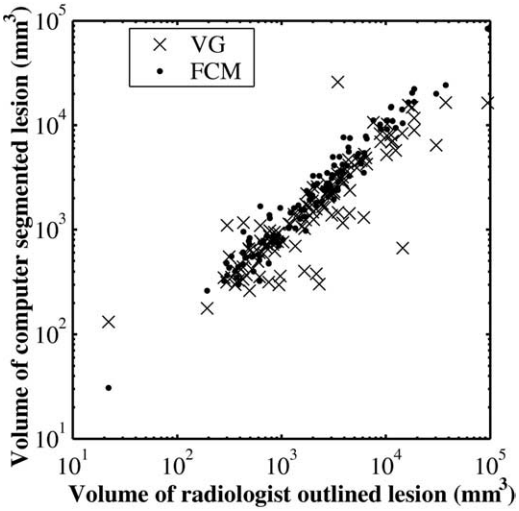

Figure 8. Relationship between lesion volumes determined from computer-segmentation and those from radiologist-outlined tumor margins for both the new FCM method (·) and our prior VG method (×). Database included 121 mass lesions.

The mean volume of lesions delineated by the radiologist was 4.7 cm^3, whereas FCM segmentation yielded a mean volume of 4.1 cm^3. Paired *t*-test was used to compare mean lesion volume measured by human delineation and FCM segmentation, and the difference was not statistically significant ($P = .71$). The correlation coefficient between human and FCM volume measurements was 0.98. The VG method yielded a mean volume of 3.0 cm^3 and a correlation coefficient of 0.64 with the radiologist's segmentation. Figure 8 is a scatter plot showing the distribution of the 121 cases based on lesion volume measured by using both the computerized methods and radiologist's outlining. It is apparent that the VG method yields more variations in results than the FCM method.

The algorithm was implemented with Matlab (Mathworks). It takes less than 1 second to segment a typical lesion on a personal computer with a 2.2-GHz AMD Athlon processor.

DISCUSSION

Why does the proposed FCM-based approach outperform the VG method? One of the key reasons might be the use of different information. In the proposed FCM-based method, all postcontrast enhancement values are used as a feature vector in differentiating between lesion and nonlesion regions. Conversely, in the VG method, VG is performed on an enhanced image in which voxel values correspond to the variance in time-weighted MR intensity values, $var_t(I(t)/t)$. Thus, enhancement values are projected to a scalar value (ie, variance), and information loss may occur in this process. In addition, in the VG method, enhancement values are weighted by the sequence number of the acquisition, which is a process that benefits the malignant lesions because malignant lesions normally show high uptake of contrast in earlier time sequences and thus are assigned a higher value in the enhanced image. To appreciate that this time-weighting process may not benefit benign lesions, it is important to note that in a typical benign lesion, signal intensity continues to increase during the time of acquisition (7,26). One might imagine an extreme situation in which signal intensity in the benign lesion increases linearly with time; then the lesion region would be assigned low values (ie, zero) in the enhanced image, and segmentation by using the VG method would be difficult. This explains the results shown in Figure 7b, in which VG performs much better in malignant than benign lesions, whereas FCM performs similarly for both malignant and benign lesions.

Normalization of postcontrast intensity by precontrast intensity is, at the first-order approximation, proportional to Gd-DTPA concentration in the extracellular space of

breast tissue (27). This is the primary reason that we used "division," rather than "subtraction," to enhance the ROIs. Another important reason is that the division operation renders the algorithm insensitive to intensity inhomogeneity artifacts. Intensity inhomogeneity corresponds to slow intensity variations of the same tissue over the image domain (28) and can be modeled as a time-invariant multiplicative gain field (29–31), namely:

$$I_{observed}(x,y,z,t) = I_{true}(x,y,z,t) \times B(x,y,z)$$

where $I_{observed}(x,y,z,t)$ and $I_{true}(x,y,z,t)$ are the observed and true MR signal intensity at voxel (x,y,z) and time t, respectively, and $B(x,y,z)$ is the bias field. The intensity in the enhanced postcontrast ROIs (Figure 4),

$$x(x,y,z,t) = \frac{I_{observed}(x,y,z,t)}{I_{obserbed}(x,y,z,0)} = \frac{I_{true}(x,y,z,t)}{I_{true}(x,y,z,0)}$$

therefore is not influenced by the bias field artifacts.

The only user input for lesion segmentation is a box-shaped ROI containing the lesion. It should be noted that the ROI is not necessarily the smallest box circumscribing the lesion, which is a requirement in some other methods (32). In practice, we found that a reasonable ROI could be specified efficiently by using the mouse on a user-friendly graphical user interface that we developed.

Patient motion during acquisition of the serial MR data may cause artifacts in enhancement. Although severe motion was not found in this data set, image registration to align images obtained at different time frames may further improve the accuracy of the segmentation.

Histological measurements of the lesions were not available for this database. We used human outlining, which was conducted very carefully by an experienced radiologist, as the "ground truth" of lesion extent. Use of the overlap measure as a performance index assumes that a method is regarded as being better if it agrees more with the radiologist. Such a philosophy is justified because tumor size estimate based on MRI interpreted by a human observer is highly accurate (8)

Automatic tumor delineation is of clinical value, for example, in surgical planning or follow-up during neoadjuvant chemotherapy. In addition, it also is important for lesion characterization, eg, in computer-based image analysis (6,7). It is expected that contrast-enhancement measures will be more stable and meaningful when applied to accurately segmented lesions. Moreover, manual outlining of the tumor on a 4D MRI data set is time intensive and impractical (may take 20–30 minutes of the radiologist's time).

Lesion segmentation is important for both benign and malignant lesions to correctly assess morphological features used to differentiate between benign and malignant lesions. Results show that the proposed FCM-based method improves the segmentation of both benign and malignant lesions, and the improvement on benign lesions is more substantial than that on malignant lesions (Figure 7b). Our ongoing research in computer-aided diagnosis of breast MRI includes extracting features from breast lesions segmented with the method presented in this report and classifying lesions as benign or malignant by merging the features by using a classifier. We expect that the improved segmentation should yield more reliable feature calculation and improved classification performance in determining the probability of malignancy.

In conclusion, we developed an FCM-based method for consistent computerized segmentation of breast lesions in three dimensions from DCE-MRI data. Performance of the proposed method is similar to performance of an experienced radiologist. The method has the potential for accurate, efficient, and consistent segmentation of breast lesions in DCE MR images.

REFERENCES

1. Schnall MD. Breast MR imaging. Radiol Clin North Am 2003; 41:43–50.
2. Heywang SH, Hahn D, Schmidt H, et al. MR imaging of the breast using gadolinium-DTPA. J Comput Assist Tomogr 1986; 10:199–204.
3. Heywang SH, Wolf A, Pruss E, Hilbertz T, Eiermann W, Permanetter W. MR imaging of the breast with Gd-DTPA: use and limitations. Radiology 1989; 171:95–103.
4. Kaiser WA, Zeitler E. MR imaging of the breast: fast imaging sequence with and without Gd-DTPA. Radiology 1989; 170:681–686.
5. Morris EA. Breast cancer imaging with MRI. Radiol Clin North Am 2002; 40:443–466.
6. Gilhuijs KGA, Giger ML, Bick U. Computerized analysis of breast lesions in three dimensions using dynamic magnetic-resonance imaging. Med Phys 1998; 25:1647–1654.
7. Chen W, Giger ML, Lan L, Bick U. Computerized interpretation of breast MRI: investigation of enhancement-variance dynamics. Med Phys 2004; 31:1076–1082.
8. Boetes C, Mus RD, Holland R, et al. Breast tumors: comparative accuracy of MR imaging relative to mammography and US for demonstrating extent. Radiology 1995; 197:743–747.
9. Davis PL, Staiger MJ, Harris KB, Ganott MA, Klementaviciene J, McCarty KS. Breast cancer measurements with magnetic resonance imaging, ultrasonography, and mammography. Breast Cancer Res Treat 1996; 37:1–9.
10. Wiberg MK, Aspelin P, Sylvan M, Bonë B. Comparison of lesion size estimated by dynamic MR imaging, mammography and histopathology in breast neoplasms. Eur Radiol 2003; 13:1207–1212.
11. Kupinski MA, Giger ML. Automated seeded lesion segmentation on digital mammograms. IEEE Trans Med Imaging 1998; 17:510–517.
12. Catarious DM, Baydush AH, Floyd CE. Incorporation of an iterative, linear segmentation routine into a mammographic mass CAD system. Med Phys 2004; 31:1512–1520.

13. Horsch K, Giger ML, Venta LA, Vyborny CJ. Automatic segmentation of breast lesions on ultrasound. Med Phys 2001; 28:1652–1659.
14. Madabhushi A, Metaxas DN. Combining low-, high-level and empirical domain knowledge for automated segmentation of ultrasonic breast lesions. IEEE Trans Med Imaging 2003; 22:155–169.
15. Lucas-Quesada FA, Sinha U, Sinha S. Segmentation strategies for breast tumors from dynamic MR images. J Magn Reson Imaging 1996; 6:753–763.
16. Gihuijs KGA, Giger ML, Bick U. A method for computerized assessment of tumor extent in contrast-enhanced MR images of the breast. In: Computer-Aided Diagnosis in Medical Imaging. Philadelphia, PA: Elsevier; 1999: 305–310.
17. Bezdek JC. Pattern Recognition With Fuzzy Objective Function Algorithm. New York: Plenum; 1981.
18. Bezdek JC, Pal SK. Fuzzy Models for Pattern Recognition. IEEE Press; NY; 1992.
19. Bezdek JC, Hall LO, Clarke LP. Review of MR image segmentation techniques using pattern recognition. Med Phys 1993; 20:1033–1048.
20. Pham DL, Prince JL. Adaptive fuzzy segmentation of magnetic resonance images. IEEE Trans Med Imaging 1999; 18:737–752.
21. Ahmed MN, Yamany SM, Mohamed N, Farag AA, Moriarty T. A modified fuzzy c-means algorithm for bias field estimation and segmentation of MRI data. IEEE Trans Med Imaging 2002; 21:193–199.
22. Baumgartner R, Windischberger C, Moser E. Quantification in functional magnetic resonance imaging: fuzzy clustering vs. correlation analysis. Magn Reson Imaging 1998; 16:115–125.
23. Jahanian H, Hossein-Zadeh G, Soltanian-Zadeh H, Ardekani BA. Controlling the false positive rate in fuzzy clustering using randomization: application to fMRI activation detection. Magn Reson Imaging 2004; 22:631–638.
24. Haralick RM, Shapiro LG. Computer and Robot Vision. Reading, MA: Addison-Wesley 1992; 1:28–48.
25. Soille P. Morphological Image Analysis: Principles and Applications. New York: Springer-Verlag; 1999; 173–174.
26. Kuhl CK, Mielcareck P, Klaschik S, et al. Dynamic breast MR imaging: are signal intensity time course data useful for differential diagnosis of enhancing lesion? Radiology 1999; 211:101–110.
27. Hoffmann U, Brix G, Knopp MV, Heb T, Lorenz WJ. Pharmacokinetic mapping of the breast: a new method for dynamic MR mammography. Magn Reson Med 1995; 33:506–514.
28. Condon BR, Patterson J, Wyper D. Image nonuniformity in magnetic resonance imaging: its magnitude and methods for its correction. Br J Radiol 1987; 60:83–87.
29. Wells WM, Grimson WEL, Kikinis R, Jolesz FA. Adaptive segmentation of MRI data. IEEE Trans Med Imaging 1996; 15:429–442.
30. Guillemaud R, Brady M. Estimating the bias field of MR images. IEEE Trans Med Imaging 1997; 16:238–251.
31. Hayton P. Analysis of Contrast-Enhanced Breast MRI. PhD dissertation. University of Oxford, Oxford, UK; 1998.
32. Penn AI, Thompson SF, Schnall MD, Loew MH, Bolinger L. Fractal discrimination of MRI breast masses using multiple segmentations. Proc SPIE Med Imaging 2000: Image Processing 2000; 3979:959–966.

Automatic identification and classification of characteristic kinetic curves of breast lesions on DCE-MRI

Weijie Chen[a)] and Maryellen L. Giger
Department of Radiology, Committee on Medical Physics, The University of Chicago, Chicago, Illinois 60637

Ulrich Bick
Department of Radiology, Charité Universitätsmedizin Berlin-Campus Charité Mitte, Berlin, Germany

Gillian M. Newstead
Department of Radiology, Committee on Medical Physics, The University of Chicago, Chicago, Illinois 60637

(Received 17 February 2006; revised 26 April 2006; accepted for publication 11 May 2006; published 24 July 2006)

Dynamic contrast-enhanced magnetic resonance imaging (DCE-MRI) of the breast is being used increasingly in the detection and diagnosis of breast cancer as a complementary modality to mammography and sonography. Although the potential diagnostic value of kinetic curves in DCE-MRI is established, the method for generating kinetic curves is not standardized. The inherent reason that curve identification is needed is that the uptake of contrast agent in a breast lesion is often heterogeneous, especially in malignant lesions. It is accepted that manual region of interest selection in 4D breast magnetic resonance (MR) images to generate the kinetic curve is a time-consuming process and suffers from significant inter- and intraobserver variability. We investigated and developed a fuzzy c-means (FCM) clustering-based technique for automatically identifying characteristic kinetic curves from breast lesions in DCE-MRI of the breast. Dynamic contrast-enhanced MR images were obtained using a T1-weighted 3D spoiled gradient echo sequence with Gd-DTPA dose of 0.2 mmol/kg and temporal resolution of 69 s. FCM clustering was applied to automatically partition the signal-time curves in a segmented 3D breast lesion into a number of classes (i.e., prototypic curves). The prototypic curve with the highest initial enhancement was selected as the representative characteristic kinetic curve (CKC) of the lesion. Four features were then extracted from each characteristic kinetic curve to depict the *maximum contrast enhancement, time to peak, uptake rate*, and *washout rate* of the lesion kinetics. The performance of the kinetic features in the task of distinguishing between benign and malignant lesions was assessed by receiver operating characteristic analysis. With a database of 121 breast lesions (77 malignant and 44 benign cases), the classification performance of the FCM-identified CKCs was found to be better than that from the curves obtained by averaging over the entire lesion and similar to kinetic curves generated from regions drawn within the lesion by a radiologist experienced in breast MRI. © *2006 American Association of Physicists in Medicine*. [DOI: 10.1118/1.2210568]

Key words: breast MRI, DCE-MRI, kinetic curve, fuzzy c-means, computer-aided diagnosis

I. INTRODUCTION

Dynamic contrast-enhanced magnetic resonance imaging (DCE-MRI) of the breast is being used increasingly in the detection and diagnosis of breast cancer as a complementary modality to mammography and sonography.[1,2] DCE-MRI offers three-dimensional spatial information and temporal information, and has demonstrated extremely high sensitivity for breast cancer.[3] The specificity of DCE-MRI, however, is varied and thus, there are continued efforts to identify distinguishing characteristics of malignant and benign lesions, including morphological features,[4–6] kinetic features,[7,8] and texture features.[9] Our study presents a new method to improve the extraction of kinetic features from DCE-MRI breast lesions, which potentially will aid radiologists in their interpretation.

Kinetic features are accessible from DCE-MRI techniques,[10–12,7,8] in which serial T1-weighted three-dimensional (3D) MR images of both breasts are acquired before and repetitively after the administration of the contrast agent gadolinium-diethylenetriamine penta-acetic acid (Gd-DTPA). The time course of the signal intensity over the lesion area is of important diagnostic value as demonstrated by Kuhl *et al.*[7] In the study by Kuhl *et al.*,[7] a kinetic curve was formed by calculating the average enhancement over a human drawn region of interest (ROI) within the lesion at all time points, where the enhancement (Eh) is defined as the percentage of signal intensity (S_t) increase relative to the precontrast signal intensity (S_0), i.e., $Eh=(S_t-S_0)/S_0$, $t=0,1,\ldots,T-1$, where T is the total number of time points. The kinetic curves were categorized into three types according to their shapes (Fig. 1): type I (persistent) curve shows continuous increase in enhancement with measurement time,

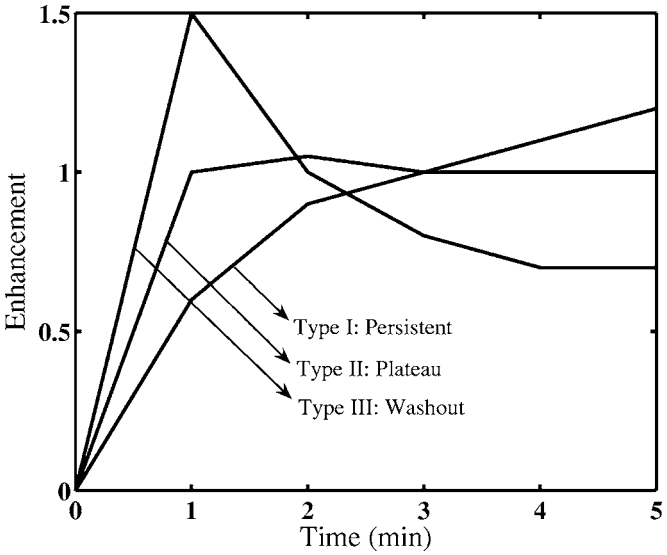

FIG. 1. Illustration of typical curve types: type I (persistent) curve shows continuous increase in enhancement with measurement time, type II (plateau) reaches a plateau, and type III (washout) exhibits a decreasing pattern after an initial increase. Enhancement (Eh) is defined as the percentage of signal intensity (S_t) increase relative to the precontrast signal intensity (S_0), i.e., $Eh=(S_t-S_0)/S_0$, $t=0,1,\ldots,T-1$, where T is the total number of time points.

type II (plateau) reaches a plateau, and type III (washout) exhibits a decreasing pattern after an initial increase. In Kuhl's study, the distributions of curve types for 101 malignant lesions and 165 benign lesions were: type I 8.9%, type II 33.6%, type III 57.4% for malignant and type I 83.0%, type II 11.5%, type III 5.5% for benign. The distributions proved to be significantly different and an overall diagnostic accuracy of 86% (sensitivity 91%, specificity 83%) was obtained.

Although the diagnostic value of kinetic curves in DCE-MRI is established, the method for generating kinetic curves is not standardized and their optimal usage has not been reached. In current clinical practice, the generation of the kinetic curves is usually done manually for each lesion in the DCE-MRI images. Typically, the radiologist or MR technologist draws a small ROI over the region that appears to be the most enhancing region in the lesion and the enhancement values at different time points are calculated over the ROI to form the kinetic curve. However, substantial interobserver variability has been reported with the manual selection of ROIs.[13] Semiautomated methods for ROI selection have been proposed in the literature.[13,14] Mussurakis *et al.*[13] compared three ROI selection methods: (a) a *large ROI* drawn by the radiologist that includes as much of the enhancing part of the lesion as possible; (b) a *small* 12-pixel circular ROI placed at the most enhancing part of the large ROI; and (c) a semiautomated ROI generated by searching within the large ROI (using a 3×3 pixel mask) for the most enhancing region. The main contribution of their study was the reported observer variability in the subjective ROI selections, and the good agreement achieved using the semiautomated ROI. Thus, semiautomated or automated ROI selection are preferred. Similar findings were reported by Liney *et al.*[14] Their semiautomated method, however, relied on a *large ROI* drawn by a human on parametric images obtained from a compartmental modeling of the dynamic data. Moreover, the choice of the size of the search mask was arbitrary, and thus difficult to optimize. In a recent study by Niemeyer *et al.*,[15] a hierarchical curve search method was proposed, in which a washout type of curve is preferably selected from curves obtained using a moving 3×3 window. While the hierarchical search technique resulted in a higher sensitivity, it was unclear if the specificity was affected.

To overcome the limitations of the methods in the literature, we propose a method based on fuzzy c-means (FCM) clustering to identify the characteristic kinetic curve (CKC) of a breast lesion in DCE-MRI images in the task of classifying the lesion as benign or malignant. Instead of searching on a parametric image using a ROI of fixed size, our method analyzes directly the signal-time curves of each voxel within the 3D lesion. FCM clustering is employed to categorize the signal-time curves into a number of prototypes (i.e., categories), and then, the prototype curve with the highest initial enhancement is automatically selected as the CKC of the lesion. Conventional kinetic features are extracted from the identified CKC and the performance of these features in distinguishing between malignant and benign lesions is evaluated with receiver operating characteristic (ROC) analysis.

II. MATERIALS AND METHODS

A. Image acquisition

In this dynamic contrast-enhanced MR imaging study, images were obtained using a T1-weighted 3D spoiled gradient echo sequence with the following parameters: repetition time (TR)=8.1 ms, echo time (TE)=4 ms, flip angle=30°. Fat suppression was not employed. The patients were scanned in prone position using a standard double-breast coil on a 1.5 T whole-body MRI system (Siemens Vision, Siemens, Erlangen, Germany). After the acquisition of the precontrast series, Gd-DTPA contrast was delivered intravenously by power injection with a dose of 0.2 mmol per kilogram body weight and a flow rate of 2 ml/s. Injection of contrast was followed by a saline flush of 20 ml with the same flow rate. Five postcontrast series were then acquired with a time interval of 69 s. Each series contained 64 coronal slices with a matrix of 128×256 pixels and an in-plane resolution of 1.25×1.25 mm^2. Slice thickness ranged from 2 to 3 mm depending on breast size.

A total of 121 patients (mean age, 51.2 years±12.7 [SD]; range, 21–85 years) with 121 primary mass lesions (77 malignant and 44 benign as revealed by biopsy) were included in this study. This database had been retrospectively collected under an IRB-approved protocol.

B. Lesion segmentation

To identify the characteristic kinetic curve of a breast lesion in DCE-MRI images, lesion segmentation must be ini-

tially performed. We investigated both a manual method and a computerized technique for the segmentation of breast lesions on the DCE-MRI images.

1. Human segmentation

The manual segmentation was performed by an experienced radiologist. This segmentation was performed slice by slice in the subtracted images (postcontrast minus precontrast). The enhanced tumor region in each slice was visually assessed and outlined by the radiologist. All subtraction images were used by the radiologist for assessing the tumor extent and the original MR images were used as additional reference.

2. Computerized segmentation

The computerized segmentation uses a fuzzy-c means (FCM)-based approach, the details of which we have reported elsewhere.[16] Briefly, the lesion segmentation algorithm consists of six consecutive stages. First, a box-shaped region of interest (ROI) containing the suspicious lesion is selected by a human operator. Then, the postcontrast ROIs are normalized by the precontrast intensities. Third, FCM clustering is applied to the normalized postcontrast time-course data to partition the voxels in the ROI into two classes: lesion and nonlesion. After binarization of the fuzzy membership map of the lesion class, a connected-component labeling operation is performed to erase the spurious structure and noise. Next, a hole-filling operation is performed on the lesion object to include the necrotic areas that have been categorized as nonlesions due to low enhancement. The performance of the computerized segmentation was evaluated by an overlap measure, which is defined as the volume of the intersection of the voxel set in radiologist-delineated lesion and the voxel set in the computer-segmented lesion over the volume of the union of the two voxel sets. At an overlap threshold of 0.4, 97% of the 121 mass lesions were correctly segmented.[16]

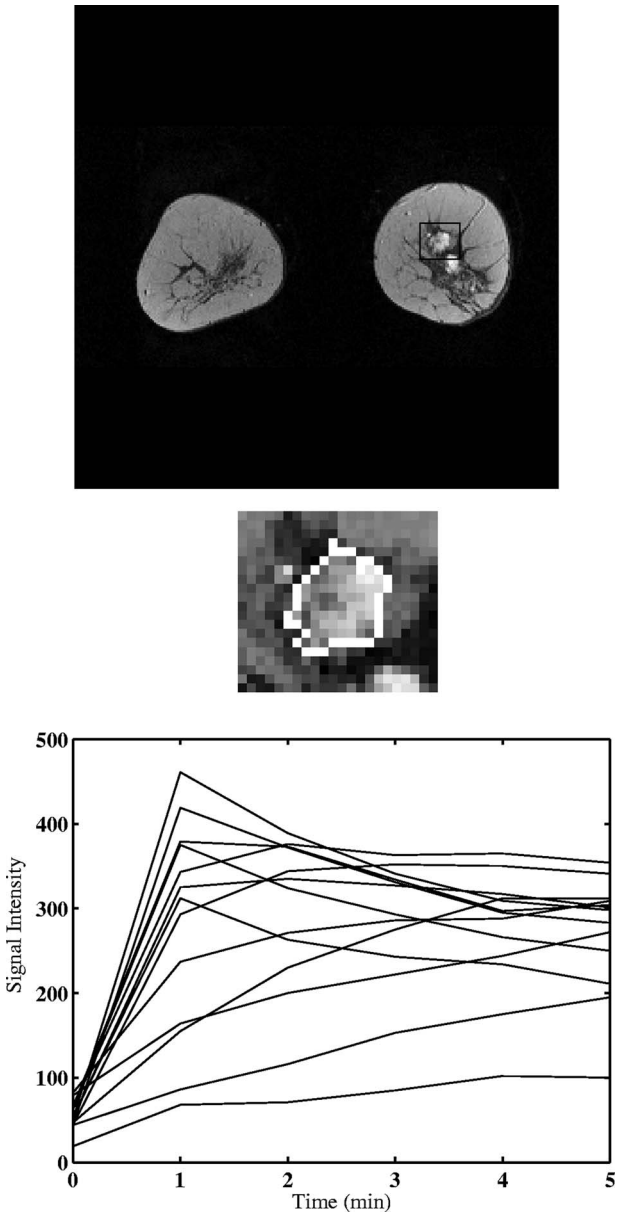

FIG. 2. Example of a breast MR image illustrating the uptake inhomogeneity in the lesion. Top: a slice containing the mass lesion. Middle: Segmented lesion with contour overlap. Bottom: signal-time curves of some randomly chosen voxels in the segmented lesion.

C. Characteristic kinetic curve identification

The inherent reason that curve identification is needed is that the uptake of contrast agent in a breast lesion is often heterogeneous, especially in malignant lesions. Figure 2 shows the signal-time curves of some randomly chosen voxels in a segmented lesion. It is apparent that all three types of kinetic curves (Fig. 1) are found in one slice of the lesion. Our method categorizes the signal-time curves in a 3D lesion into a number of prototypes and selects the one that best represents the lesion for diagnosis purpose, i.e., the most enhancing curve. We propose using this fuzzy c-means (FCM) clustering[17,18] technique to identify the curve prototypes.

Denote N as the number of voxels in a suspicious lesion. Each voxel is represented by signal intensity values at all the time points. Thus, we have data set

$$X = \{\mathbf{x}_i, i = 1,2, \ldots, N | \mathbf{x}_i = (S_{i0}, S_{i1}, \ldots, S_{i,T-1})\}, \quad (1)$$

where $\mathbf{x_i}$ is the data vector for the ith voxel, $S_{it}(t = 0,1,\ldots,T-1)$ is the signal intensity of the ith voxel at time point t, and T is the number of time points. In FCM clustering, we attempt to partition the data set X into c classes, where c is a parameter to be specified. The prototypic curves corresponding to the (unknown) classes are represented by a $c \times T$ matrix V; the kth $(k=1,2,\ldots,c)$ row of V, $\mathbf{v_k}$, is a T-dimensional vector representing the prototypic curve of the kth class. The (fuzzy) partition of the data set is represented by a $c \times N$ matrix U. The element of U, u_{ki}, represents the membership of the ith data point $(\mathbf{x_i})$ to the kth class $(\mathbf{v_k})$ and characterizes the similarity between the ith data point $(\mathbf{x_i})$

and the kth class prototype ($\mathbf{v_k}$). The FCM objective function to be minimized is

$$J(U,V;X)=\sum_{k=1}^{c}\sum_{i=1}^{N}u_{ki}^{b}\|\mathbf{x}_i-\mathbf{v_k}\|, \tag{2}$$

with the following constraints:

$$\sum_{k=1}^{c}u_{ki}=1,\ \forall i;\quad 0\leqslant u_{ki}\leqslant 1,\ \forall k,i;\quad \sum_{i=1}^{N}u_{ki}>0,\ \forall k, \tag{3}$$

where $b\in[1,\infty)$ is a weighting exponent on each fuzzy membership, and $\|\cdot\|$ denotes the Euclidean distance. The necessary conditions for the FCM objective function in Eq. (2) to be minimized with the constraints in (3) can be derived by LaGrange multipliers,

$$u_{ki}=\frac{1}{\sum_{l=1}^{c}\left(\frac{\|\mathbf{x_i}-\mathbf{v_k}\|}{\|\mathbf{x_i}-\mathbf{v_l}\|}\right)^{2/(b-1)}},\quad k=1,2,\ldots,c;\quad i=1,2,\ldots,N, \tag{4}$$

$$\mathbf{v_k}=\frac{\sum_{i=1}^{N}u_{ki}\mathbf{x_i}}{\sum_{i=1}^{N}u_{ki}^{b}},\quad k=1,2,\ldots,c. \tag{5}$$

In implementation, matrix V is randomly initialized, and then U and V are obtained through an iterative process using Eq. (4) and Eq. (5). The convergence criterion of the iteration is that the Euclidean distance between the current prototype matrix and the prototype matrix in the previous iteration is less than some user-specified number ϵ, i.e., $\|V_{\text{new}}-V_{\text{old}}\|<\epsilon$.

Note that the number of classes c in FCM clustering must be a known parameter. We empirically determined the parameter c from the number of voxels in a lesion as follows:

$$c=\begin{cases}[N/80] & \text{if } N>160\\ 2 & \text{if } N\leqslant 160,\end{cases} \tag{6}$$

where [ ] takes the nearest integer. The parameter fuzzy index b was set to $b=2$ and the convergence criteria parameter $\epsilon=10^{-5}$.

After one obtains V, i.e., c prototypic curves, the curve with the maximum initial enhancement is selected as the characteristic kinetic curve of the lesion,

$$k=\arg\max_{j=1,2,\ldots,c}\frac{v_{j1}-v_{j0}}{v_{j0}}. \tag{7}$$

Thresholding of the corresponding membership map, i.e., the kth row of matrix U, can be used to label the most enhancing regions.

The algorithm is summarized as follows:

(1) Empirically specify the number of classes in a lesion with Eq. (6);
(2) Initialize V randomly;
(3) Update U with Eq. (4);
(4) Update V with Eq. (5);
(5) If $\|V_{\text{new}}-V_{\text{old}}\|<\epsilon$ go to 3, otherwise go to 6; and
(6) Select curve using Eq. (7).

Figure 3 illustrates the curve identification procedure. In Fig. 3(a), 3D breast MR images (first postcontrast series) are displayed as multiple slices, with a malignant mass lesion segmented by a radiologist. Figure 3(b) shows the color-encoded membership map overlapped on the original lesion, marking the most enhancing regions in the lesion and (c) shows all the FCM-detected prototypic curves in the lesion. The characteristic kinetic curve (CKC) selected using the criterion in (7) is displayed in (d) (solid line). Also shown is the curve obtained by averaging over the entire lesion (dash line).

D. Feature extraction

To classify the lesions as malignant or benign, four features are extracted from the CKC of each lesion. Note that each CKC was represented by the signal intensity values at T time points, $(S_0,S_1,\ldots,S_{T-1})$, where S_t is the signal intensity at time point $t(t=0,1,\ldots,T-1)$. Denoting S^* as the maximum of the T signal intensity values and p as the time point of S^*, i.e.,

$$S^*=\max_{t=0,1,\ldots,T-1}S_t, \tag{8}$$

$$p=\arg\max_{t=0,1,\ldots,T-1}S_t. \tag{9}$$

The four features extracted are defined as follows:

(1) Maximum enhancement (F_{k1}),

$$F_{k1}=(S^*-S_0)/S_0, \tag{10}$$

(2) Time to peak (F_{k2}),

$$F_{k2}=p, \tag{11}$$

(3) Uptake rate (F_{k3}),

$$F_{k3}=\frac{F_{k1}}{F_{k2}}, \tag{12}$$

(4) Washout rate (F_{k4}),

$$F_{k4}=\begin{cases}\dfrac{S^*-S_{T-1}}{S_0(T-1-p)} & \text{if } p\neq T-1\\ 0 & \text{if } p=T-1.\end{cases} \tag{13}$$

E. Evaluation

We assessed the performance of the four kinetic features (defined above in Sec. II D.) in the task of distinguishing between malignant and benign lesions using ROC analysis.[19,20] To demonstrate the usefulness of our technique, we used the ROCKIT ROC software[21] to compare the classification performance of the features extracted from the CKC identified using our method with: (1)the features extracted from the kinetic curve obtained by averaging over the entire

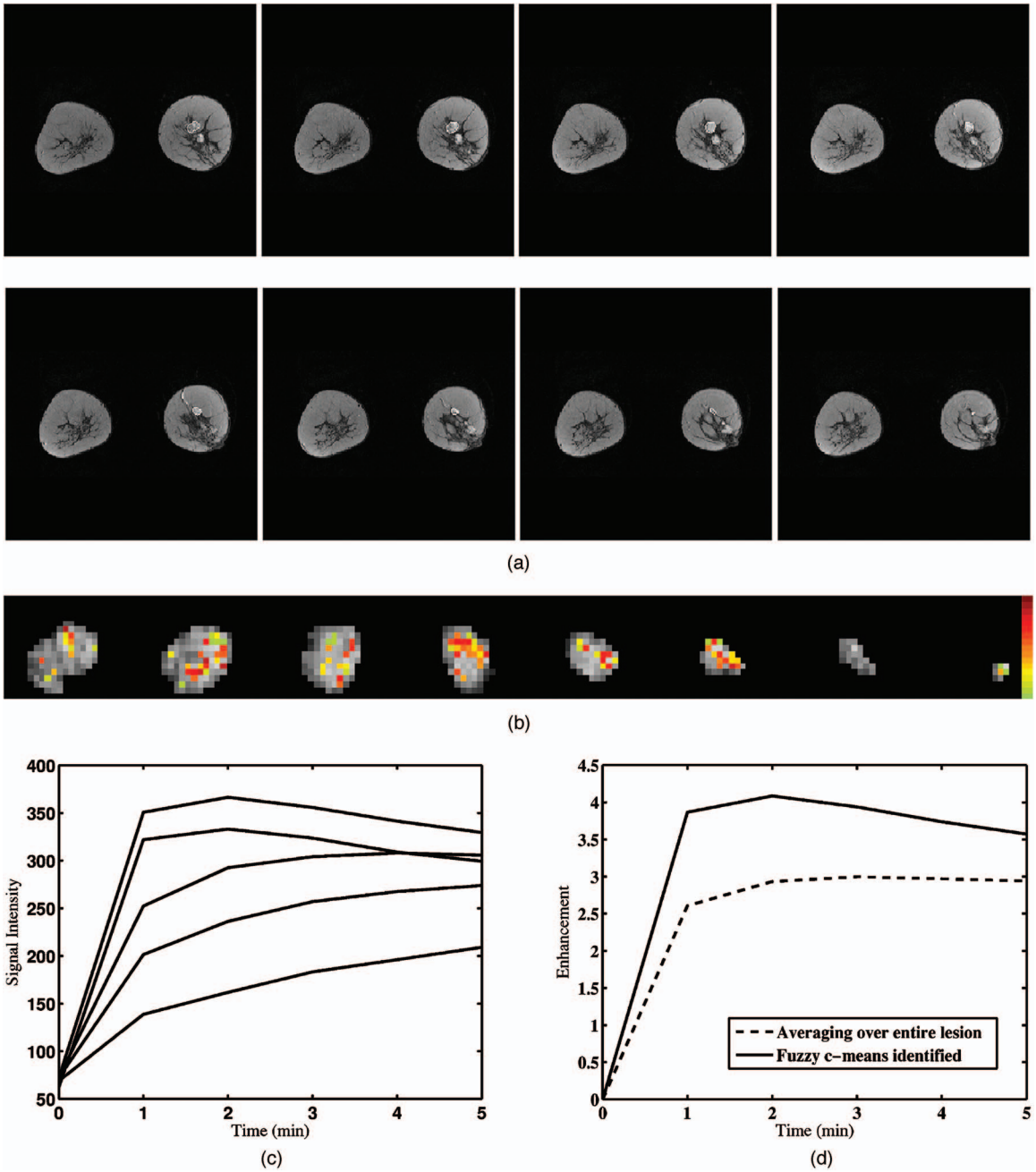

FIG. 3. Illustration of the curve identification method. (a) 3D breast MR images (first postcontrast series) displayed as multiple slices, with a malignant mass lesion segmented by a radiologist. (b) Color-encoded membership map overlapped to the original lesion marking the most enhancing regions in the lesion. (c) Detected prototype curves within the lesion; (d) The characteristic kinetic curve identified by our FCM clustering method (solid line) and the curve obtained by averaging over the radiologist-outlined lesion region (dash line).

lesion; and (2)the features extracted from the kinetic curve generated from a manually selected small region within the lesion. The regions were selected by a radiologist experienced in breast MRI (U.B.) without knowledge of the clinical information or diagnosis. The regions were drawn using a self-developed software tool allowing the definition of arbitrarily shaped regions. While drawing the regions, both pre- and postcontrast images as well as subtraction images were available. Regions were placed in a representative area of strong initial enhancement.

III. RESULTS

Figures 4 and 5 show examples of curve identification for malignant and benign cases, respectively. In each plot, the kinetic curve obtained by averaging over the entire lesion (dashed line, referred to as "average curve") and the characteristic kinetic curve identified by our FCM clustering method (solid line, referred to as "CKC") are displayed. For the malignant examples in Fig. 4, the average curves in (a)–(c) exhibit a persistent type and the CKCs show plateau or

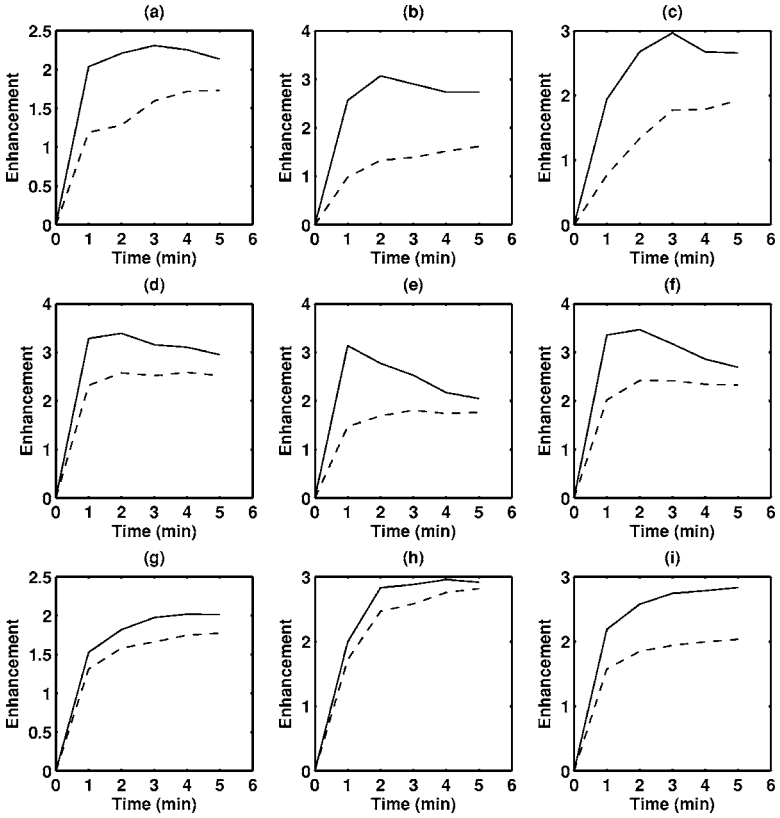

FIG. 4. Malignant examples. In each plot, the dashed line represents the curve obtained by averaging over the entire lesion, and the solid line represents the characteristic kinetic curve identified automatically by our FCM clustering-based method.

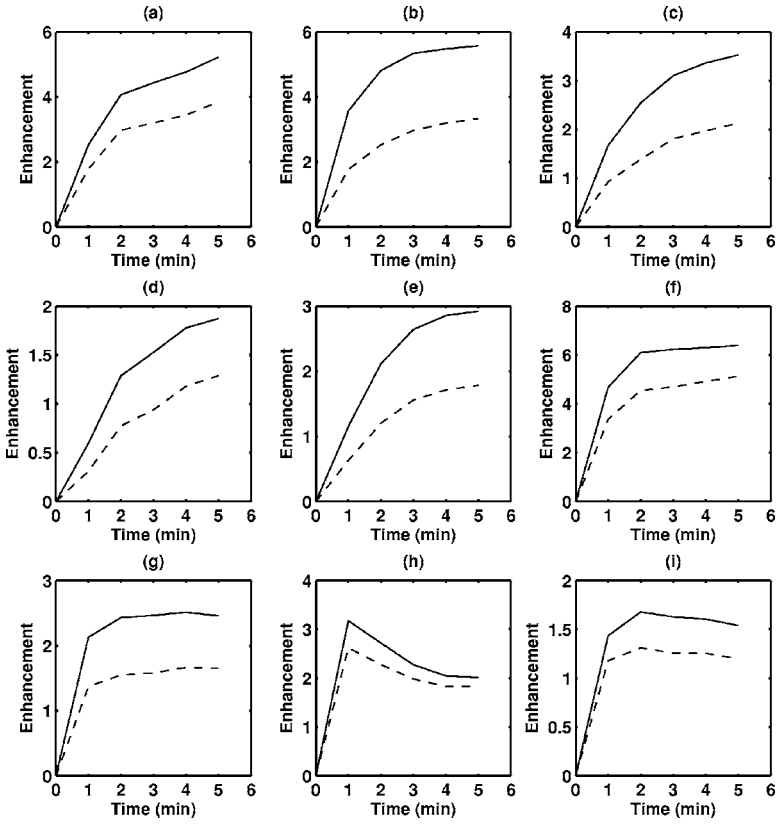

FIG. 5. Benign examples. Same convention as Fig. 4.

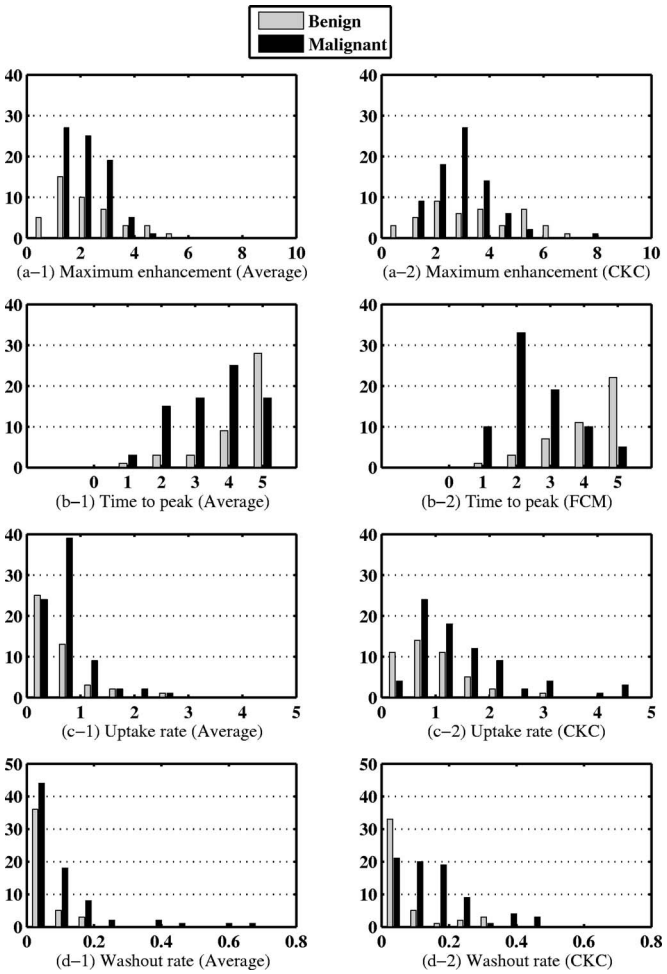

FIG. 6. Histograms of feature values for the database for the kinetic curves averaged over the entire lesion (left column) and for the automatically identified characteristic kinetic curves using our FCM-based method (right column).

washout; the average curves in (d)–(f) exhibit a plateau while the CKCs show washout. For these examples, the estimated likelihood of malignancy increased when the FCM method was employed. However, Figures 4(g) and 4(h) show some malignant examples whose average curves and CKCs are similar. Figure 4(i) shows a rare example where the average curve demonstrates a plateau type while the CKC exhibits a persistent type. For the benign examples shown in Fig. 5, both the average curves and the CKCs in (a)–(f) demonstrate the typical persistent type, and both the average curves and the CKCs in (g)–(i) show nontypical washout or plateau types. This suggests that use of the proposed FCM method will increase, in general, the malignant kinetic appearance of cancerous lesions while not affecting that of benign lesions.

Figure 6 shows histograms of the kinetic features of the malignant and benign cases in the database derived from both the average curve (left column) and the CKCs (right column). These histograms demonstrate the changes in the feature distributions and in the separations between the malignant and benign groups as the kinetics analysis changes from the average curves to the CKCs. Overall, the maximum enhancement increases for both the benign and malignant lesions due to the use of CKCs. However, an increase in the separation between the two groups is not observed [Figs. 6(a-1) and 6(a-2)]. For the last three features, CKCs yielded greater separation between the malignant group and benign group as compared to that from the corresponding average curves. CKCs tend to reach the peak earlier than average curves, especially with the malignant lesions [Figs. 6(b-1) and 6(b-2)]. From Figs. 6(c) and 6(d), it is evident that more cases from the malignant group than from the benign group yield increased uptake rates and washout rates with CKCs as compared to those from the corresponding average curves.

TABLE I. Comparison of classification performance of kinetic features: "FCM" means that the features are extracted from FCM-identified characteristic kinetic curves; "Average" means that the features are extracted from kinetic curves generated by averaging over the entire lesion. The lesions were initially outlined by an experienced radiologist (U.B).

	A_z (FCM)	A_z (Average)	p value	95% CI of ΔA_z
Max. enhancement	0.55±0.06	0.55±0.06	0.98	(–0.22, 0.22)
Time to peak	0.85±0.04	0.76±0.05	0.008	(0.02, 0.15)
Uptake rate	0.71±0.05	0.66±0.06	0.19	(–0.02, 0.12)
Washout rate	0.80±0.05	0.74±0.05	0.14	(–0.02, 0.12)

Quantitative results of the classification performance of kinetic features, in terms of area under the ROC curve, are summarized in Tables I–III. In all these comparisons, the A_z values (i.e., area under the ROC curve), p values for statistical comparison of two methods, and the 95% confidence interval (CI) of the difference in A_z values are given.

Table I shows the comparison of classification performance of kinetic features extracted from FCM-identified CKCs with that from the average curves from the initial radiologist outlined lesions. The feature maximum enhancement is of little discriminatory power for both methods. For the other three features—time to peak, uptake rate, and washout rate—the A_z values based on the FCM-identified curves are higher than that based on the average curves. The difference in A_z values for the feature time to peak is statistically significant.

Table II lists the comparison of classification performance of kinetic features extracted from FCM-identified CKCs with that from the curves generated from radiologist-drawn regions within the lesions. Again, the feature maximum enhancement is of little discriminatory power for both methods.

TABLE II. Comparison of classification performance of kinetic features: "FCM" means that the features are extracted from FCM-identified characteristic kinetic curves; "MAN" means that the features are extracted from kinetic curves generated from regions drawn manually by a radiologist experienced in breast MRI.

	A_z (FCM)	A_z (MAN)	p value	95% CI of ΔA_z
Max. enhancement	0.57±0.06	0.50±0.06	0.09	(–0.01, 0.14)
Time to peak	0.85±0.04	0.79±0.05	0.11	(–0.02, 0.14)
Uptake rate	0.71±0.05	0.74±0.05	0.48	(–0.11, 0.05)
Washout rate	0.79±0.05	0.71±0.05	0.04	(0.01, 0.15)

TABLE III. Comparison of classification performance of kinetic features: "Human outline" means that the FCM-based curve identification was performed on radiologist-outlined breast lesions; "computer segmentation" means that the FCM-based curve identification was performed on the computer-segmented breast lesions.

	A_z (Human outline)	A_z (computer seg.)	p value	95% CI of ΔA_z
Max. enhancement	0.57±0.06	0.56±0.06	0.80	(−0.04, 0.05)
Time to peak	0.85±0.04	0.85±0.04	0.76	(−0.04, 0.03)
Uptake rate	0.71±0.05	0.71±0.05	0.96	(−0.04, 0.03)
Washout rate	0.79±0.05	0.78±0.05	0.51	(−0.02, 0.04)

The A_z values of the features time to peak and uptake rate are similar for the two methods. The A_z value for the feature washout rate extracted from FCM-identified CKCs is significantly higher than that from curves generated from the radiologist-drawn regions.

It should be noted that the automatic curve identification using our FCM-based method is performed on breast lesions segmented either by computer or human. Table III compares the classification performance of the kinetic features based on curves obtained from human-outlined breast lesions and that based on the curves obtained from the computer-segmented breast lesions. We failed to show a significant difference between the human outlining and the computer segmentation for all the four features.

IV. DISCUSSION AND CONCLUSION

We investigated and developed a fuzzy c-means clustering-based technique for automatically identifying characteristic kinetic curves of breast lesions in DCE-MRI. FCM was applied to partition the signal-time curves obtained for each voxel in a segmented 3D breast lesion, into a number of prototypic curves, and the curve with the highest initial enhancement was automatically selected as the characteristic kinetic curve of the lesion. Four features were extracted from each CKC to depict the maximum enhancement, time to peak, uptake rate, and washout rate of the lesion kinetics. The classification performance of these features in the task of distinguishing between benign and malignant lesions was assessed by ROC analysis. The area under the ROC curve from the FCM-identified CKCs was higher than that from the curves obtained by averaging over the entire lesion, and this improvement was found to be statistically significant for the feature time to peak.

We also compared the classification performance of the kinetic features extracted from FCM-identified CKCs with that from curves generated from radiologist-drawn regions within the lesion. The A_z values are similar for two of the kinetic features (time to peak and uptake rate) and FCM-identified CKCs yielded significant higher A_z value for the feature washout rate. It is worth noting that the interpretation of the kinetic curves is not standardized in the current clinical practice. We basically used our computerized features to evaluate the classification performance of kinetic curves obtained with different methods. To best simulate a clinical environment, we also compared the performance of a kinetic feature used by one of the radiologists (U.B.). Note that each kinetic curve was represented by the signal intensity values at T time points $(S_0, S_1, \ldots, S_{T-1})$, where $S_t(t=0,1,\ldots,T-1)$ is the signal intensity at time point t. The empirical decision variable is based on the ratio between late and early enhancement, and is defined as

$$F_k = \frac{S_{T-1} - S_1}{S_1 - S_0}.$$

This decision variable is negative for kinetic curves with washout, zero for kinetic curves with a plateau, and positive for kinetic curves with continuous enhancement. This feature yielded an A_z value of 0.85 (s.e. 0.04) for the FCM-identified characteristic kinetic curves and an A_z value of 0.81 (s.e. 0.05) for the curves generated from radiologist-drawn regions. We failed to observe a significant difference between the two A_z values. However, it is accepted that manual ROI selection in 4D breast MR images is a time-consuming process and suffers from significant inter- and intraobserver variability.[13]

One of the significant aspects of the results in Table III is that computerized segmentation[16] yielded essentially the same A_z values as did the human segmentation. This implies that, once the lesion is located, the characteristic kinetic curve can be obtained automatically without radiologist's interaction. There are two advantages associated with this automated lesion-segmentation process. First, the objectivity of the analysis is increased since the interobserver variability in lesion outlining is avoided; and second, the efficiency of the analysis is increased since the slice-wise human delineation of 3D breast lesions is time-consuming and impractical in actual clinical practice.

The number of prototypic curves (c) to be detected in a lesion must be a known parameter to apply the FCM clustering technique. Intuitively, when c is too small, the identified curves will be close to the average curve and less characteristic. When c is too large, however, curve identification may be sensitive to noise. We used a rule in Eq. (6) to specify the parameter c as the number of voxels in the 3D breast lesion divided by 80. The optimal selection of this parameter requires a larger database and is beyond the scope of this study.

The most enhancing regions associated with the identified characteristic kinetic curve, as shown in the color map in Fig. 3(b), convey interesting information. These most enhancing areas might be irregularly shaped and even spatially disconnected within a 3D breast lesion. This fact may render it questionable to generate a curve with a regular-shaped size-fixed window.

It should be noted that there are still no standardized and generally accepted protocols for breast MR imaging. However, there is considerable agreement among radiologists about suitable MR imaging techniques.[22–24,1,2] For example, dedicated double-surface coils are indispensable, and high magnetic field and strong gradients should be used for improved contrast enhancement. Also, T1-weighted three-dimensional gradient echo-pulse sequences are used for dy-

namic breast MR imaging for 6 to 10 min following bolus injection of Gd-DTPA. Typically one precontrast and a series of postcontrast images of both breasts at a temporal resolution of 60 to 90 s are acquired. The dost of the contrast agent is generally between 0.1 and 0.2 mmol per kilogram body weight. The spatial resolution is approximately 1 mm in all planes and slice thickness is approximately 2 mm with no gap. The MRI protocol used in our study is similar to these protocols. Historically, mainly due to technical limitations, high temporal resolution protocol was used by sacrificing spatial resolution and vice versa (the so-called "dynamic school" and "static school" as summarized in a review by Kuhl *et al.*[22]). More recently, both high spatial resolution and high temporal resolution imaging were reported in a multicenter study.[25] In their study, 3D T1-weighted high spatial resolution images were first acquired before and after the administration of Gd-DTPA. Then, a progression saturation data set was obtained to estimate the T1 relaxation time followed by an acquisition of 2D high temporal resolution (15 s) dynamic contrast-enhanced series.

Of interest is the the applicability of our proposed method to the varying MR imaging protocols. The proposed method essentially consists of two stages: curve identification and curve classification. The FCM-based curve identification method is a data-oriented, model-free approach. The method is motivated by the within-lesion uptake heterogeneity properties and does not make any assumptions about the temporal resolution. Therefore, the curve identification method is in general applicable to any dynamic study. However, improved temporal resolution has the potential to improve the classification performance. The curve classification method uses four conventional kinetic features based on the MR signal enhancement, which is a relative measure of the contrast uptake. MRI protocols, in which T1 relaxation time measurements are available, can estimate the contrast concentration at each voxel from the dynamic data using compartmental modeling.[26,27] Features based on contrast concentration kinetics and permeability parameters extracted using compartmental modeling could potentially improve the classification performance.

Patient motion during acquisitions of different MR data series may introduce inaccuracies in kinetic curves; however nonrigid image registration techniques[28–30] can be used to correct for such motion. In our study, abrupt and large patient movements between dynamic series were not found, and only patient respiratory motion was observed. The motion mostly resulted in additional blurring rather than actual displacement of image structure (e.g., most enhancing regions). However, it is important to note that image alignment of breast volumes at different time frames is expected to improve the accuracy of our analyses.

Overall, the proposed approach for automatically identifying characteristic kinetic curve has the potential to increase the objectivity and efficiency of breast MR image interpretation. It is important to note that, while we were focusing on the kinetic aspect of the breast MRI interpretation in this study, breast MRI interpretation and diagnostic decision rely on a combination of both kinetic and architectural features.[1,2,31] We are investigating a computerized classification scheme that combines both kinetic and architectural features to distinguish between benign and malignant breast lesion in DCE-MRI. We believe that the automatic method proposed in this study for kinetic curve generation and kinetic feature extraction will be a key component in our computerized classification scheme.

ACKNOWLEDGMENTS

The authors would like to thank Lorenzo Pesce, Ph.D., and Michael R. Chinader, Ph.D., for useful discussions on ROC analysis. This work is supported in part by DOD Breast Cancer Research Program Predoctoral Traineeship Award (Grant DAMD17-03-1-0245), Lawrence H. Lanzl Graduate Student Fellowship in Medical Physics (Committee On Medical Physics, The University of Chicago) and USPHS Grant CA89452. M. L. Giger is a shareholder in R2 Technology, Sunnyvale, CA. It is the policy of the University of Chicago that investigators disclose publicly actual or potential significant financial interests that may appear to be affected by the research activities.

[a]Electronic mail: weijie@uchicago.edu

[1]E. A. Morris, "Breast cancer imaging with MRI," Radiol. Clin. North Am. **40**, 443–466 (2002).
[2]M. D. Schnall, "Breast MR imaging," Radiol. Clin. North Am. **41**, 43–50 (2003).
[3]P. J. Kneeshaw, L. W. Turnbull, and P. J. Drew, "Current applications and future direction of MR mammography," Br. J. Cancer **88**, 4–10 (2003).
[4]L. W. Nunes, M. D. Schnall, S. G. Orel, M. G. Hochman, C. P. Langlotz, and C. A. Reynolds, "Breast MR imaging: Interpretation model," Radiology **202**, 833–841 (1997).
[5]L. W. Nunes, M. D. Schnall, and S. G. Orel, "Update of breast MR imaging architectural interpretation model," Radiology **219**, 484–494 (2001).
[6]K. G. A. Gilhuijs, M. L. Giger, and U. Bick, "Computerized analysis of breast lesions in three dimensions using dynamic magnetic-resonance imaging," Med. Phys. **25**, 1647–1654 (1998).
[7]C. K. Kuhl, P. Mielcareck, S. Klaschik, C. Leutner, E. Wardelmann,J. Gieseke, and H. H. Schild, "Dynamic breast MR imaging: Are signal intensity time course data useful for differential diagnosis of enhancing lesion?" Radiology **211**, 101–110 (1999).
[8]W. Chen, M. L. Giger, L. Lan, and U. Bick, "Computerized interpretation of breast MRI: Investigation of enhancement-variance dynamics," Med. Phys. **31**, 1076–1082 (2004).
[9]P. Gibbs and L. W. Turnbull, "Textural analysis of contrast-enhanced MR images of the breast," Magn. Reson. Med. **50**, 92–98 (2003).
[10]S. H. Heywang-Köbrunner, D. Hahn, H. Schmidt, I. Krischke, W. Eiermann, R. Bassermann, and J. Lissner, "MR imaging of the breast using gadolinium-DTPA," J. Comput. Assist. Tomogr. **10**, 199–204 (1986).
[11]S. H. Heywang-Köbrunner, A. Wolf, E. Pruss, T. Hilbertz, W. Eiermann, and W. Permanetter, "MR imaging of the breast with gd-DTPA: Use and limitations," Radiology **171**, 95–103 (1989).
[12]W. A. Kaiser and E. Zeitler, "MR imaging of the breast: Fast imaging sequence with and without gd-DTPA," Radiology **170**, 681–686 (1989).
[13]S. Mussurakis, D. L. Buckley, and A. Horsman, "Dynamic MRI of invasive breast cancer: Assessment of three region-of-interest analysis methods," J. Comput. Assist. Tomogr. **21**, 431–438 (1997).
[14]G. P. Liney, P. Gibbs, C. Hayes, M.O. Leach, and L. W. Turnbull, "Dynamic contrast-enhanced MRI in the differentiation of breast tumors: User-defined versus semiautomated region-of-interest analysis," J. Magn. Reson Imaging **10**, 945–949 (1999).
[15]T. Niemeyer, C. Wood, K. Stegbauer, and J. Smith, "Comparison of automatic time curve selection methods for breast MR CAD," in *Proceedings SPIE, Medical Imaging 2004: Image Processing* (2004), Vol. 5370,

pp. 785–790.
[16]W. Chen, M. L. Giger, and U. Bick, "A fuzzy c-means (FCM) based approach for computerized segmentation of breast lesions in dynamic contrast-enhanced MR images," Acad. Radiol. **13**, 63–72 (2006).
[17]J. Bezdek, *Pattern Recognition with Fuzzy Objective Function Algorithm* (Plenum, New York, 1981).
[18]J. Bezdek and S. K. Pal, *Fuzzy Models for Pattern Recognition* (IEEE, Piscataway, NJ, 1992).
[19]C. E. Metz, "Some practical issues of experimental design and data analysis in radiological ROC studies," Invest. Radiol. **24**, 234–245 (1989).
[20]C. E. Metz, B. A. Herman, and C. A. Roe, "Statistical comparison of two ROC-curve estimates obtained from partially-paired datasets," Med. Decis Making **18**, 110–121 (1998).
[21]C. E. Metz, "ROCKIT (computer program), version 0.9b, 1998." Available from http://www-radiology.uchicago.edu/krl/roc_soft.htm
[22]C. K. Kuhl and H.H. Schild, "Dynamic image interpretation of MRI of the breast," J. Magn. Reson Imaging **12**, 965–974 (2000).
[23]T. H. Helbich, "Contrast-enhanced magnetic resonance imaging of the breast," Eur. J. Radiol. **34**, 208–219 (2000).
[24]S. H. Heywang-Köbrunner, U. Bick, W. G. B., Jr, B. Bon, J. Casselman, A. Coulthard, U. Fischer, M. Mller-Schimpfle, H. Oellinger, R. Patt, J. Teubner, M. Friedrich, G. Newstead, R. Holland, A. Schauer, E. A. Sickles, L. Tabar, J. Waisman, and K.D. Wernecke, "International investigation of breast MRI: Results of a multicentre study (11 sites) concerning diagnostic parameters for contrast-enhanced MRI based on 519 histopathologically correlated lesions," Eur. Radiol. **11**, 531–546 (2001).
[25]M. D. Schnall, J. Blume, D.A. Bluemke, G. A. DeAngelis, N. DeBruhl, S. Harms, S. H. Heywang-Köbrunner, N. Hylton, C. K. Kuhl, E. D. Pisano, P. Causer, S. J. Schnitt, D. Thickman, C. B. Stelling, P. T. Weatherall, C. Lehman, and C. A. Gatsonis, "Diagnostic architectural and dynamic features at breast MR imaging: Multicenter study," Radiology **238**, 42–53 (2006).
[26]P. S. Tofts and A.G. Kermode, "Measurement of the blood-brain barrier permeability and leakage space using dynamic MR imaging. I. Fundamental concepts," Magn. Reson. Med. **17**, 357–367 (1991).
[27]U. Hoffmann, G. Brix, M. V. Knopp, T. Heb, and W. J. Lorenz, "Pharmacokinetic mapping of the breast: A new method for dynamic MR mammography," Magn. Reson. Med. **33**, 506–514 (1995).
[28]D. Rueckert, L. I. Sonoda, C. Hayes, D. L. G. Hill, M. O. Leach, and D. J. Hawkes, "Non-rigid registration using free-form deformations: Application to breast MR images," IEEE Trans. Med. Imaging **18**, 712–721 (1999).
[29]T. Rohlfing, C. R. Maurer, D.A. Bluemke, and M. A. Jacobs, "Volume-preserving nonrigid registration of MR breast images using free-form deformation with an incompressibility constraint," IEEE Trans. Med. Imaging **22**, 730–741 (2003).
[30]X. Chen, M. Brady, J. L.-C. Lo, and N. Moore, "Simultaneous segmentation and registration of contrast-enhanced breast MRI," in *Information Processing in Medical Imaging: 19th International Conference, IPMI 2005, Glenwood Springs, CO, USA, July 10-15, 2005. Proceedings*, edited by G. E. Christensen and M. Sonka (Springer, Berlin, 2005), Vol. 3565, pp. 126–137.
[31]M. D. Schnall and D.M. Ikeda, "Lesion diagnosis working group on breast MR," J. Magn. Reson Imaging **10**, 982–990 (1999).

Volumetric texture analysis of DCE-MR images of the breast using gray-level co-occurrence matrix method

W. Chen[1], M. L. Giger[1]

[1]Radiology, The University of Chicago, Chicago, IL, United States

Introduction

Texture analysis using 2D-image-based gray level co-occurrence matrix method [1] has been demonstrated to be useful in distinguishing between malignant and benign breast lesions in contrast-enhanced MR images [2]. 2D texture analysis does not take advantage of the 3D data in breast MR images and requires high signal-to-noise ratio, which may not be available in dynamic studies. We hypothesize that an overall assessment of texture on the accurately segmented 3D breast lesions would yield improved differentiation performance than 2D analysis. We extend the conventional 2D texture analysis technique to 3D in the framework of gray-level co-occurrence matrix method, and assess the performance of textural features in the task of distinguishing between malignant and benign breast lesions.

Materials and Methods

Our database consists of 77 malignant lesions and 44 benign lesions. Dynamic contrast-enhanced magnetic resonance (DCE-MR) images were obtained using a T1-weighted 3D spoiled gradient echo sequence (TR = 8.1 ms, TE = 4 ms, flip angle = 30^0). The patients were scanned in the prone position using a standard double breast coil on a 1.5 T whole-body MRI system. After the acquisition of the precontrast series, Gd-DTPA contrast agent was delivered intravenously by power injection with a dose of 0.2 mmol/kg and a flow rate of 2 ml/s. Five postcontrast series were taken with a time interval of 69 s. Each series contained 64 coronal slices with a matrix of 128×256 pixels and an in-plane resolution of 1.25 mm × 1.25 mm. Slice thickness ranged from 2.0 mm to 3.0 mm depending on breast size.

We extend the conventional concept of 2D-image-based gray level co-occurrence matrix (GLCM) to 3D image. The difference of spatial locations of two voxels is described by a displacement vector $\mathbf{d} = (d_x, d_y, d_z)$. For an image of G gray levels, the $G \times G$ gray level co-occurrence matrix P_d for a displacement vector $\mathbf{d}$ is defined as follows. The entry (i, j) of P_d is the number of occurrence of voxel pair of gray levels i and j whose spatial locations are a vector $\mathbf{d}$ apart. In 3D, there are 13 independent directions corresponding to 26 displacement vectors (Figure 1).

We initially segmented the 3D breast lesions in DCE-MRI using an automatic approach that we previously developed [3]. Bilinear interpolation was performed on the first postcontrast image data to make the voxels isotropic. The lesion data were then equal-probability quantized into 128 gray levels. For each lesion, 13 gray level co-occurrence matrices were calculated from the quantized postcontrast data and added together to get a non-directional GLCM. Then 11 features related to second-order statistics [1] were calculated from the GLCM. The performance of each feature in the task of distinguishing between malignant and benign lesions was assessed using receiver operating characteristic (ROC) analysis [4]. The area under ROC curve (A_z) was used as a performance index.

Results and Discussion

For the 11 texture features under investigation, 7 features yielded statistically significant higher A_z values when 3D analyses were used than when 2D analyses were used (Table 2). We failed to show significant differences between 3D and 2D for the other four feautres. In conclusion, 3D texture analysis based on accurately segmented 3D breast lesions improved diagnostic accuracy as compared to 2D texture analyses based on 2D ROIs.

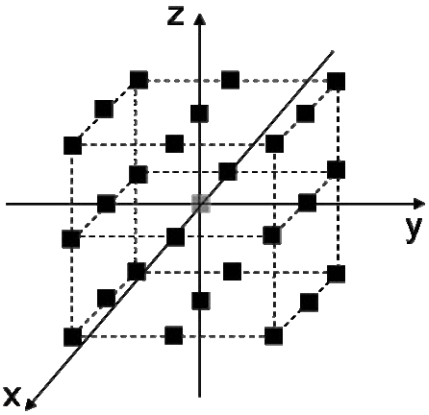

Figure 1. Illustration of 26 voxel pairs (gray and black) in 3D image space.

Acknowledgement

This work is supported by DOD Breast Cancer Research Program grant DAMD17-03-1-0245 and USPHS grant CA89452

References

[1]. Haralick RM et al. *IEEE Trans Syst Man Cybernet* 1973; **3**: 610-621.
[2]. Gibbs P et al. *Magn. Reson. Med* 2003;. **50**:92-98
[3]. Chen W et al. *Acad. Radiol.* 2006; in press
[4]. Metz CE et al. *Med Decis Making* 1998; **18**: 110-121.

Table 1. Comparison of A_z values for 11 features in 3D and 2D texture analysis

(DE-difference entropy, DV-difference variance, IDM-inverse difference moment, SA-sum average, SE-sum entropy, SV-sum variance)

feature	contrast	correlation	DE	DV	Energy	Entropy	IDM	SA	SE	SV	variance
A_z (2D)	.51	.53	.52	.56	.59	.60	.55	.67	.62	.62	.77
A_z (3D)	.76	.69	.72	.76	.62	.65	.52	.62	.79	.86	.85
p	**0.006**	**.0005**	**.0001**	**$<10^{-4}$**	.66	.41	.76	.16	**.009**	**.0001**	**.02**